# NIST BUILDING SCIENCE SERIES 173

# Heat and Moisture Transfer in Wood-Based Wall Construction: Measured Versus Predicted

R. R. Zarr, D. M. Burch and A. H. Fanney

Building and Fire Research Laboratory
National Institute of Standards and Technology
Gaithersburg, MD 20899-0001

February 1995


**U.S. Department of Commerce**
Ronald H. Brown, *Secretary*

**Technology Administration**
Mary L. Good, *Under Secretary for Technology*

**National Institute of Standards and Technology**
Arati Prabhakar, *Director*

National Institute of Standards and Technology Building Science Series 173
Natl. Inst. Stand. Technol. Bldg. Sci. Ser. 173, 83 pages (Feb. 1995)
CODEN: NBSSES

U.S. GOVERNMENT PRINTING OFFICE
WASHINGTON: 1995

For sale by the Superintendent of Documents, U.S. Government Printing Office, Washington, DC 20402–9325

# ABSTRACT

The National Institute of Standards and Technology has developed a personal computer program, MOIST, that predicts the transient one-dimensional heat and moisture transfer in building envelopes. MOIST allows the user to vary building materials, their relative placement within the building envelope, and the geographic location of the building. For a given geometry and location, it predicts the resulting moisture accumulation and transfer across each construction layer as a function of time.

This report describes a comprehensive laboratory study to verify the accuracy of MOIST for 12 different wall specimens. The rate of heat transfer through each of the 12 wall specimens was measured. The moisture content of the exterior construction materials were measured for eight of the twelve wall specimens. For the remaining four walls, the relative humidity level was measured at the interior side of the exterior sheathing. The measured heat transfer rates, moisture content levels and relative humidities were compared to the predictions of MOIST.

In general, the agreement between MOIST and the experimental measurements was good. The moisture content predicted by MOIST was within one percent of the measured values for seven of the eight walls that contained moisture content sensors. The measured relative humidities for two of the remaining four walls agreed well with the MOIST predictions. The relative humidity measurements from the other two walls could not be compared to MOIST since the walls were constructed with vapor retarder defects that introduced two-dimensional effects. The heat flux predicted by MOIST was within ten percent of the values measured under steady-state conditions. When the walls were subjected to a series of diurnal ambient temperature cycles, the root-mean-square difference between the measured and predicted heat flux values ranged from four to fifteen percent. MOIST heat flux predictions were also in close agreement with the values predicted by the Thermal Analysis Research Program (TARP).

A comparison was made between measured steady-state thermal resistances and corresponding calculated values using procedures recommended by The American Society of Heating, Refrigerating, and Air Conditioning Engineers (ASHRAE). The ASHRAE calculations agreed with the measured values within thirteen percent.

**Keywords**

apparatus; building science; building technology; calibrated hot box; computer models; experiment; heat transfer; mass transfer; MOIST; moisture transfer; relative humidity; temperature; thermal resistance; validation; wall

# TABLE OF CONTENTS

# TABLE OF CONTENTS (continued)

# LIST OF FIGURES

## LIST OF FIGURES (continued)

# LIST OF TABLES

# NOMENCLATURE

| | |
|---|---|
| a | constant in Equation (9), $W/(m^2 \cdot K^{(4/3)})$ |
| A | cross-sectional area, $m^2$ |
| $A_0$ | constant coefficient for heat flux transducer function, $W/m^2$ |
| $A_1$ | linear coefficient for heat flux transducer function, $W/(m^2 \cdot mV)$ |
| b | constant in Equation (9), $W \cdot s/(m^3 \cdot K)$ |
| $B_{1,2,3}$ | coefficients for sorption-isotherm function |
| $c_p$ | specific heat of air at constant pressure, $J/(kg \cdot K)$ |
| $C_{1,2,3}$ | coefficients for permeability function |
| $D_0$ | coefficient for thermal-conductivity function, $W/(m \cdot K)$ |
| $D_1$ | coefficient for thermal-conductivity function, $W \cdot m^2/(kg \cdot K)$ |
| $D_2$ | coefficient for thermal-conductivity function, $W \cdot kg/(m^4 \cdot K)$ |
| emf | electromotive force, mV |
| exp | exponential function |
| $G_t$ | total water vapor transfer resistance, $Pa \cdot m^2 \cdot s/kg$ |
| $h_c$ | convective conductance of vertical airspace $W/(m^2 \cdot K)$ |
| $h_i$ | inside air film coefficient, $W/(m^2 \cdot K)$ |
| $h_o$ | outside air film coefficient, $W/(m^2 \cdot K)$ |
| $h_w$ | water vapor permeance of vertical airspace $kg/(s \cdot m^2 \cdot Pa)$ |
| j | index |
| J | number of layers of building materials |

## NOMENCLATURE (continued)

| | |
|---|---|
| ln | natural logarithm function |
| L | thickness of specimen, m |
| Le | Lewis number |
| m | slope of best-fit of water vapor resistance data, s·m·Pa/kg |
| MC | moisture content, percent |
| n | index |
| N | number of points |
| $P_{atm}$ | atmospheric pressure, Pa |
| $P_g$ | saturation water vapor pressure, Pa |
| $P_{gv}$ | water vapor pressure inside glass vessel, Pa |
| $P_v$ | water vapor pressure inside glass vial, Pa |
| q | heat flux, $W/m^2$ |
| Q | power, W |
| $R_j$ | thermal resistance of layer j, $m^2 \cdot K/W$ |
| $R_{HFT}$ | measured thermal resistance of wall, $m^2 \cdot K/W$ |
| $R_T$ | overall calculated thermal resistance of wall, $m^2 \cdot K/W$ |
| RH | relative humidity, percent |
| RMS | root-mean-square |
| RSD | residual standard deviation of fit, $W/m^2$ |
| s | standard deviation |
| t | elapsed time, s |

## NOMENCLATURE (continued)

| | |
|---|---|
| $T_m$ | mean temperature between surface and surrounding radiant environment, K |
| $T_i$ | measured inside air temperature, °C |
| $T_o$ | measured outside air temperature, °C |
| U | calculated thermal transmittance of wall, $W/(m^2 \cdot K)$ |
| $v_{air}$ | velocity of air film, m/s |
| V | output voltage of heat flux transducer, mV |
| w | water vapor transfer rate, kg/s |
| $\delta_{RMS}$ | root-mean-square difference, percent moisture content |
| $\Delta_n$ | difference between measured and predicted moisture content, percent moisture content |
| $\Delta\phi$ | relative humidity difference, percent |
| $\Delta T$ | temperature difference between hot and cold plates, °C |
| $\Delta T_{air}$ | temperature difference across air film, °C |
| $\Delta T_t$ | temperature difference across wall specimen at time t, K |
| $\epsilon$ | surface emittance |
| $\lambda$ | (apparent) thermal conductivity, $W/(m \cdot K)$ |
| $\mu$ | permeability, $kg/(s \cdot m \cdot Pa)$ |
| $\phi$ | relative humidity |
| $\rho$ | density, $kg/m^3$ |
| $\sigma$ | Stefan-Boltzmann constant, $W/(m^2 \cdot K^4)$ |
| $\Sigma$ | summation operator |

# INTRODUCTION

Guidelines are needed for controlling moisture in building envelopes. Current moisture control practices are based upon the geographic location of the building, the construction materials used, field study results, and local experience. The existing guidelines and practices are often debated by experts in the building community and, for the most part, unsupported by analysis. For example, most practitioners recommend that an interior vapor retarder be installed in building envelopes. In a cold climate, an interior vapor retarder impedes the ingress of moisture from the indoor environment, thereby minimizing potentially damaging moisture accumulation in the sheathing and siding of walls. However, this same practice is counterproductive in a wall of an air conditioned house located in a hot and humid climate. In this situation, moisture from the outdoor environment permeates through the wall construction and accumulates at the interior vapor retarder. Failure to properly control moisture within a building envelope may lead to increased energy usage, degradation of building materials, and the growth of biological agents such as fungal spores (Bales and Rose 1991).

Field studies have provided valuable information for documenting specific moisture problems for a given type of building construction in a specific climate. Field studies have also provided an understanding of the underlying physics involved in the transfer of heat and moisture through building components. However, despite the valuable information that field studies provide, it is difficult to generalize the results of a given field study to different building materials, climates, and indoor environmental conditions. Moreover, it is impractical to implement the number of field studies which would be required to address all possible combinations of construction types and climatic conditions.

The National Institute of Standards and Technology (NIST) has developed a personal computer program, MOIST (Burch and Thomas 1993) which provides the means for developing appropriate moisture control guidelines. MOIST predicts the transient heat and moisture transfer in building envelopes having multi-layer construction under nonisothermal conditions. MOIST solves the one-dimensional conservation of energy and conservation of mass equations using the finite-difference method. MOIST allows the user to vary building materials, their relative placement within the building envelope, and the geographic location of the building. It includes transfer of moisture in the diffusion and the capillary flow regimes. The vapor-transfer resistance of paint layers and vapor retarders is readily included. Outdoor weather conditions are available for 51 cities (Crow 1981). The program calculates and plots the average moisture content of the layers of construction versus time of year for a given set of indoor and outdoor conditions.

As is the case with any model, MOIST requires verification by comparison to laboratory experiments as well as field studies. This report describes a comprehensive laboratory study conducted by NIST to verify the accuracy of MOIST.

# EXPERIMENT

## Overview

Twelve wall specimens were built and tested collectively in the NIST calibrated hot box. The calibrated hot box was operated continuously for 104 days providing nominal conditions of 21 °C and 50 percent relative humidity at the interior surfaces of the wall specimens and a range of ambient temperatures and relative humidities at the exterior surfaces. For the first 42 days, the interior and exterior surfaces were preconditioned at roughly the same conditions of 21 °C and 50 percent relative humidity. After preconditioning, the exterior temperature was decreased suddenly to 7.2 °C for one day. For the next 6 days, a series of diurnal sinewaves were imposed on the exterior surfaces in which the amplitude of the air temperature varied from 1.1 to 15.6 °C. The exterior temperature was then maintained at a nominal air temperature of 7.2 °C for 34 days. For seven days, the exterior surfaces were exposed again to a second series of diurnal sinewaves having nearly the same boundary conditions as the first series. Finally, the exterior temperature was elevated to a nominal temperature of 32 °C for the last 14 days.

During the experiment, the moisture content and temperature of selected exterior materials, the heat flux through each wall specimen, and the ambient air temperatures and relative humidities were measured. The measured moisture contents were subsequently compared to values predicted by MOIST simulations of the experiment. These simulations used the experimental boundary conditions and independently measured material properties, such as the water vapor sorption isotherm and permeance, as input data. The measured heat flux through each wall specimen was compared to the values predicted by MOIST simulations and also values calculated from procedures in the ASHRAE Handbook of Fundamentals (ASHRAE 1993). The calculated values of heat flux were determined using the measured thermal conductivity for the materials within the wall specimens.

## Wall Specimens

Twelve wall specimens were constructed within the 300-mm thick frame of the NIST calibrated hot box, Figure 1. Each specimen had overall dimensions of 1.0 by 1.1 m and was designed with a centrally located meter section, 305 mm in diameter. In designing each wall specimen, finite-element calculations were conducted to insure that the heat transfer through each specimen was one-dimensional. To minimize lateral transport of moisture between the meter section and surrounding materials, the meter section was circumscribed by a thin 0.03-mm sleeve of polycarbonate-plastic film as shown in Figure 2. The specimens consisted of either three or four layers of building materials typical of residential wood-frame construction, namely: gypsum wallboard; cavity insulation of glass fiber or loose-fill cellulose; sheathing of either fiberboard, fir plywood, or foil-faced polyisocyanurate; and siding of sugar pine or vinyl. The building materials were obtained locally and are described in Appendix A.

WALL SPECIMEN LOCATION WITHIN CALIBRATED HOT BOX
(Exterior View)

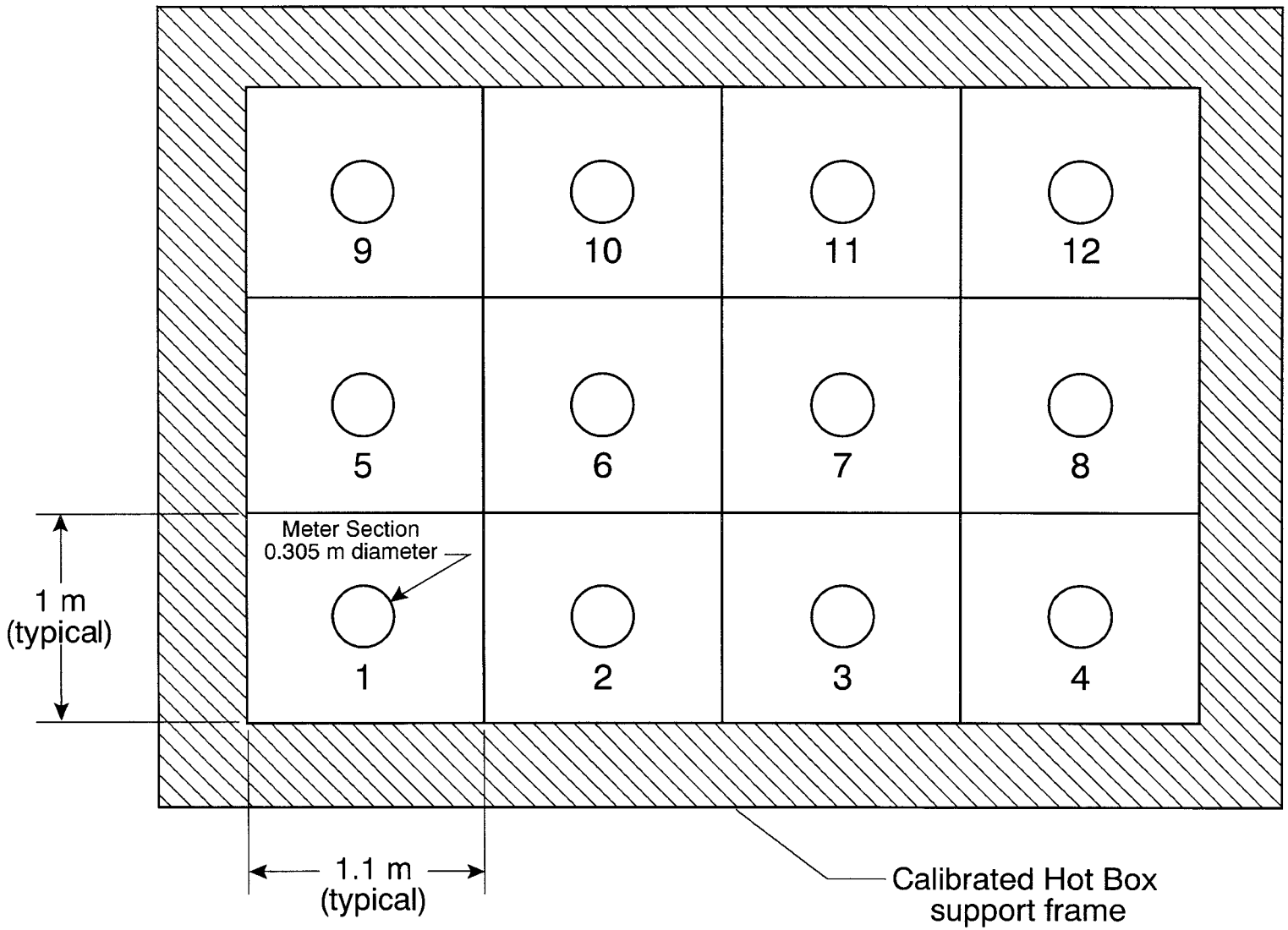


Figure 1

# METER SECTION CONSTRUCTION DETAILS

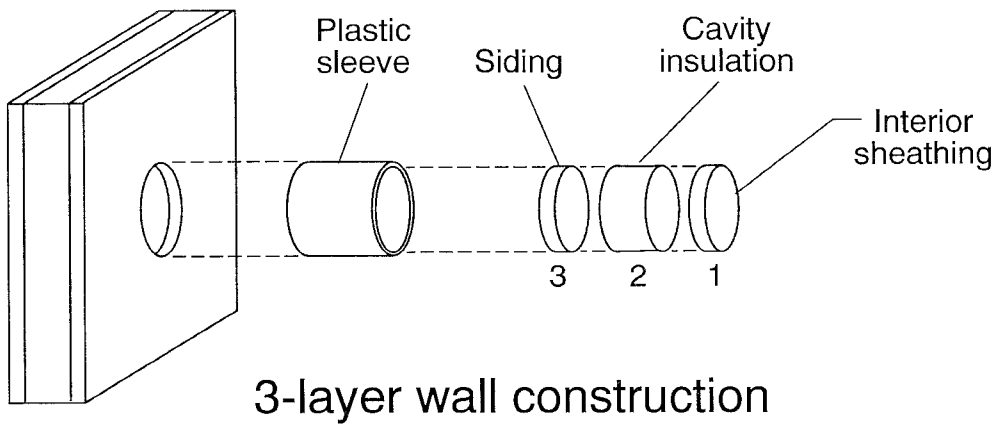


3-layer wall construction

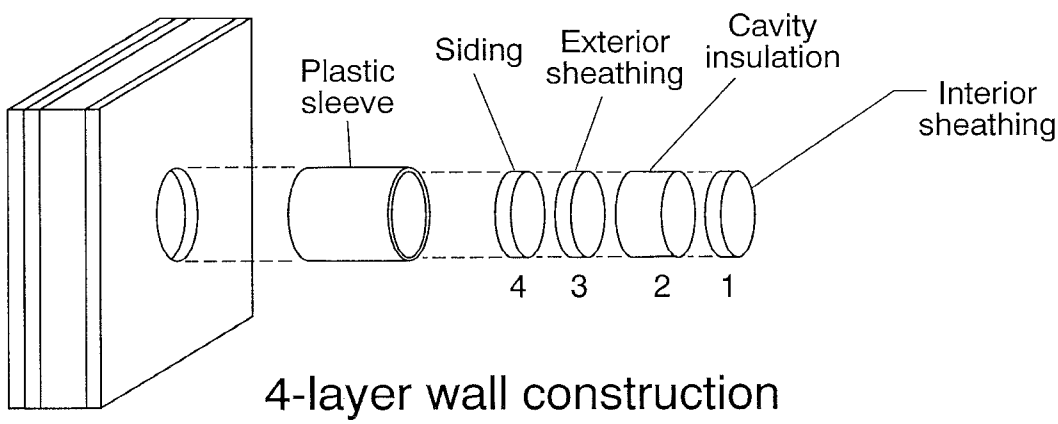


4-layer wall construction

Figure 2

Construction details and a material list for each wall specimen are illustrated in Figure 3. The first eight wall specimens were designed specifically for verification of MOIST. These specimens utilized a design strategy that varied a single parameter of construction from specimen-to-specimen. For example, specimen 1 was constructed with three layers of materials: gypsum wallboard, glass-fiber insulation, and sugar pine siding. Specimens 2 through 8 varied one item of construction; 2, added a vapor retarder; 3, interior latex paint and exterior oil paint; 4, interior and exterior latex paint; 5, fiberboard sheathing; 6, plywood sheathing; 7, cavity airspace; and, 8, cellulose insulation. This strategy examined the relative effects of each of these parameters on the movement of moisture through the specimens.

The four other specimens, 9 to 12, were more representative of current building practices and were designed to explore the effectiveness of a vapor retarder on moisture movement. Again, a single parameter of construction was varied. Specimens 10 and 11 were the same construction as 9, except both were constructed purposely with a defect. The defect consisted of a 11.5-mm-diameter hole in specimen 10 and a 7.9-mm-diameter hole in specimen 11. The diameter of each hole was determined from design data compiled on effective leakage areas for electric outlets in the ASHRAE Handbook of Fundamentals (ASHRAE 1993). Note that specimen 12 was the same as specimen 9 except the vapor retarder was excluded. A summary of the wall specimen constructions is presented in Table 1.

# WALL SPECIMEN CONSTRUCTION DETAILS

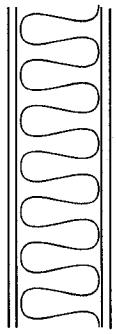

1.
Gypsum board
Glass-fiber insulation
Sugar pine

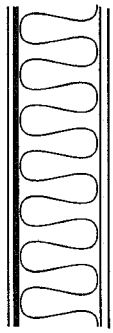

2.
Gypsum board
Glass-fiber insulation
w/asphalt -kraft paper
Sugar pine

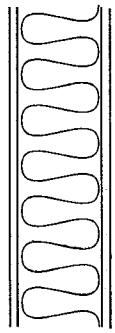

3.
Latex paint
Gypsum board
Glass-fiber insulation
Sugar pine
Oil paint

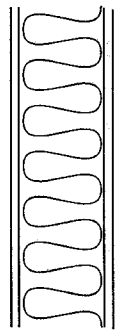

4.
Latex paint
Gypsum board
Glass-fiber insulation
Sugar pine
Latex paint

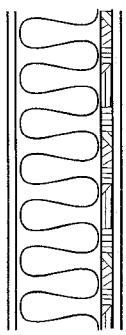

5.
Gypsum board
Glass-fiber insulation
Fiberboard sheathing
Sugar pine

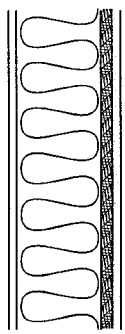

6.
Gypsum board
Glass-fiber insulation
Plywood sheathing
Sugar pine

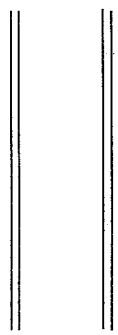

7.
Gypsum board
Air - space
Sugar pine

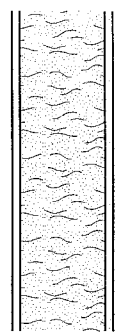

8.
Gypsum board
Cellulose insulation
Sugar pine

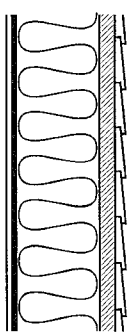

9.
Latex paint
Gypsum board
Glass-fiber insulation
w/ asphalt - kraft paper
Foil-faced polyisocyanurate
Vinyl

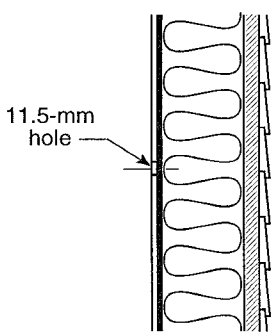


10.
Latex paint
Gypsum board
Glass-fiber insulation
w/ asphalt - kraft paper
Foil-faced polyisocyanurate
Vinyl

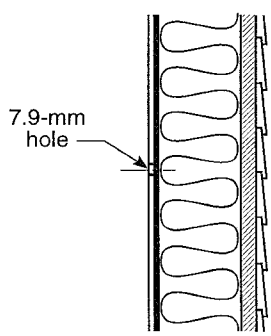


11.
Latex paint
Gypsum board
Glass-fiber insulation
w/ asphalt - kraft paper
Foil-faced polyisocyanurate
Vinyl

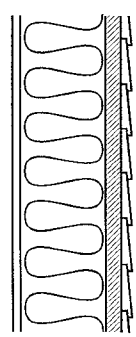

12.
Latex paint
Gypsum board
Glass-fiber insulation
Foil-faced polyisocyanurate
Vinyl

Figure 3

**Table 1**
**Wall Specimen Constructions**

| Materials | Nominal Thickness (mm) | Specimen | | | | | | | | | | | |
|---|---|---|---|---|---|---|---|---|---|---|---|---|---|
| | | 1 | 2 | 3 | 4 | 5 | 6 | 7 | 8 | 9 | 10[1] | 11[2] | 12 |
| 1. Interior latex paint[3] | - | | | x | x | | | | | x | x | x | x |
| 2. Gypsum wallboard | 12.7 | x | x | x | x | x | x | x | x | x | x | x | x |
| 3. Glass-fiber insulation | 81.4 | x | | x | x | x | x | | | | | | x |
| 4. Glass-fiber insul., w/vapor retarder | 81.4 | | x | | | | | | | x | x | x | |
| 5. Cellulose loose-fill insulation | 81.4 | | | | | | | | x | | | | |
| 6. Airspace | 81.4 | | | | | | | x | | | | | |
| 7. Fiberboard sheathing | 12.7 | | | | | x | | | | | | | |
| 8. Plywood sheathing (fir) | 12.7 | | | | | | x | | | | | | |
| 9. Foil-faced polyisocyanurate foam | 12.7 | | | | | | | | | x | x | x | x |
| 10. Sugar pine siding | 19.1 | x | x | x | x | x | x | x | x | | | | |
| 11. Vinyl siding | - | | | | | | | | | x | x | x | x |
| 12. Exterior latex paint[3] | - | | | | x | | | | | | | | |
| 13. Exterior oil paint[3] | - | | | x | | | | | | | | | |

[1] One hole, 11.5-mm-diameter, was placed purposely in the center of the meter section.
[2] One hole, 7.9-mm-diameter, was placed purposely in the center of the meter section.
[3] One coat primer and one coat finish applied after the heat flux and moisture-content sensors were installed.

## Calibrated Hot Box

A schematic of NIST's calibrated hot box is given in Figure 4. The NIST calibrated hot box complies with the American Society for Testing and Materials Test Method C 976 (ASTM 1994). The apparatus consists of three principal components: a metering chamber, a climatic chamber, and a specimen support frame. These components were designed to provide controlled conditions of temperature, air flow, and radiation on each side of the wall specimen and to measure the resulting heat flow through the wall specimen. In this study, the calibrated hot box was operated in a manner which provided controlled temperature and relative humidity conditions at the interior and exterior surfaces of the wall specimens. A detailed description of the facility is available in the literature (Achenbach, P.R. 1979, Zarr et al. 1987) and a brief review of the components is given below.

The metering chamber consists of a five-sided, highly-insulated, enclosure. Its exterior walls are comprised of rigid polyurethane insulation, 381 mm thick, providing a thermal resistance of R-16 $m^2 \cdot K/W$. Surrounding the exterior surface of the rigid polyurethane insulation is a chilled-water guard maintained at the same temperature as the air in the metering chamber. The chamber walls are finished with a thin (1.7 mm) sheet of reinforced fiber-glass plastic. Due to the large thermal resistance of the walls and the small temperature gradient, the rate of heat transfer through the chamber walls is quite small i.e., less than 0.5 W (Zarr et al. 1987).

Air within the metering chamber was circulated at a constant rate by a propeller-type fan and conditioned by an electric heater and a cooling coil. The cooling coil was operated at a constant chilled-water flow rate and was operated at a temperature above 10 °C. A platinum-resistance thermometer measured the dry-bulb temperature within the metering chamber. The relative humidity of the air was controlled by humidifying the supply air with a vaporizer and measured using a thin-film capacitance humidity sensor. Conditioned air was delivered to the top of the specimen through air diffusers designed to deliver a uniform distribution of air across the specimen. The baffle wall was coated with flat-black paint to provide a total hemispherical emittance greater than 0.8.

The climatic chamber consists of a five-sided enclosure, the same size and configuration as the metering chamber, except its walls are constructed without an external chilled-water guard. The thickness of the rigid polyurethane insulation is 457 mm, providing a thermal resistance of R−19 $m^2 \cdot K/W$. The chamber walls are also finished with a thin sheet of reinforced fiber-glass plastic.

Conditioned air for the climatic chamber was provided by one of two external systems as shown in Figure 4. For dry conditions, air was conditioned by an electric heater and a refrigeration system. A portion of the air was diverted to a two-stage rotating-drum desiccant dryer that removed water vapor from the air. The dryer maintained a low dew point, preventing frost from diminishing the capacity of the refrigeration coil. For humid conditions, the refrigeration system and desiccant dryer were not used and air was instead conditioned by a heated vaporizer and a chilled-water cooling coil. The dry-bulb temperature and relative humidity within the climatic

# SCHEMATIC OF THE NIST CALIBRATED HOT BOX

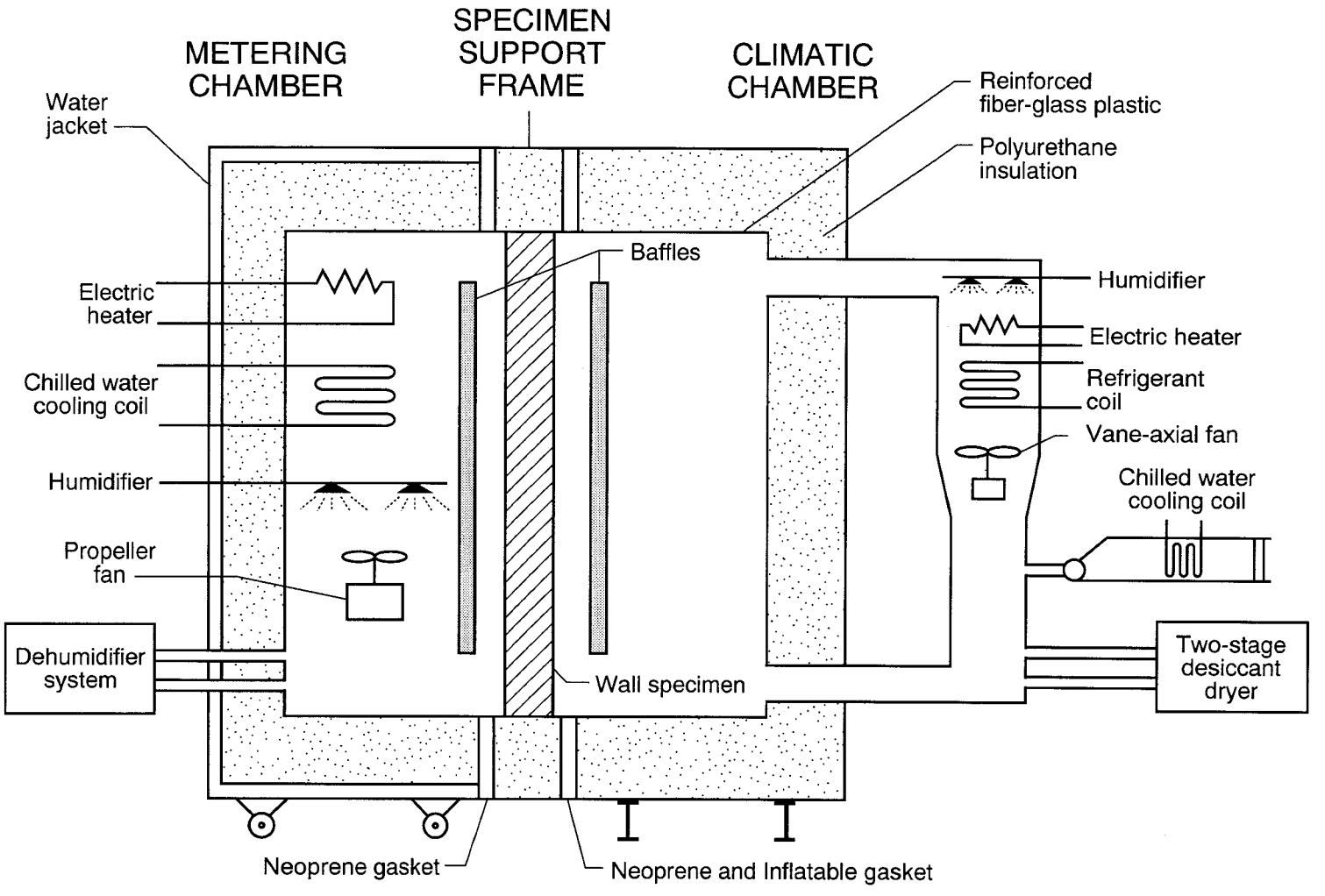


Figure 4

chamber were measured using a platinum-resistance thermometer and thin-film capacitance humidity sensor, respectively. The humidity level within the climatic chamber was controlled manually. Conditioned air was circulated to the climatic chamber by a vane-axial fan and delivered to the bottom of the specimen through air diffusers. The baffle wall was coated with flat-black paint to provide a total hemispherical emittance greater than 0.8.

The 300-mm-wide specimen frame can support wall specimens having a thickness of 250 mm and an overall area of 3.0 by 4.6 m. The frame is comprised of 457-mm-thick rigid polyurethane insulation finished with a thin 1.7-mm sheet of plastic reinforced fiber-glass plastic to provide a vapor barrier. The design was engineered to minimize the heat transfer through the specimen frame and provide structural support for the specimen.

## Data Acquisition

The data-acquisition system consists of a portable computer interfaced to a data acquisition system. The computer controls the data acquisition system, converts the sensor signals into engineering quantities, corrects the measurements using calibration data, averages the data over appropriate time intervals, displays the current measurements on a video monitor, and records the data on a disk.

## Boundary Conditions

During the experiment, the metering chamber maintained a steady indoor condition of 21.2 $\pm$ 0.1 °C and 50 $\pm$ 3 percent relative humidity at the interior surfaces of the wall specimens. The airspeed moving past the interior surfaces was maintained at 0.4 m/s in a downward direction. During this same period, the climatic chamber provided the ambient conditions shown in Figure 5 at the exterior surfaces of the wall specimens. At the exterior surfaces, the air speed was maintained at 1.0 m/s in an upward direction. The sequence of ambient conditions in the climatic chamber is summarized in Table 2.

**Table 2**
**Climatic Chamber Conditions**

| Condition | Days |
|---|---|
| Pre-Conditioning | 42 |
| Winter - Steady | 1 |
| Winter - Diurnal Sinewave | 6 |
| Winter - Steady | 34 |
| Winter - Diurnal Sinewave | 7 |
| Summer - Steady | 14 |

# CLIMATIC CHAMBER BOUNDARY CONDITIONS

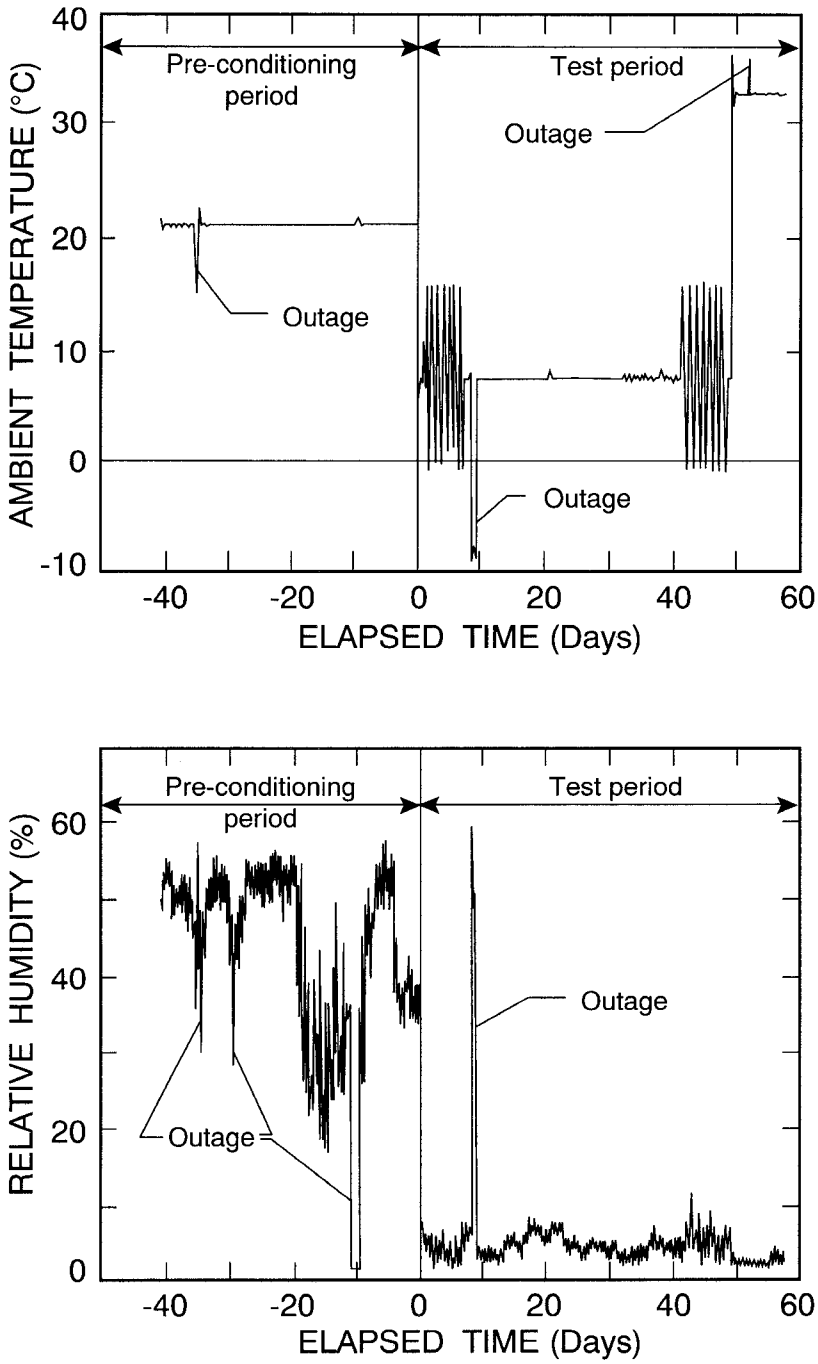


Figure 5

The wall specimens were initially pre-conditioned in order to establish initial moisture contents within the construction materials. The test period was partitioned into four winter periods and one summer period. At the end of the pre-conditioning period, the ambient temperature within the climatic chamber was reduced quickly to 7.2 °C for one day in preparation for the first series of diurnal sinewaves. The purpose of the first series of diurnal sinewaves was to investigate the time-dependent transfer of heat and moisture when the wall specimens were comparatively dry. During the second steady winter period, moisture migrated through the wall specimens and accumulated in the hygroscopic sheathing and siding materials. The purpose of the second series of diurnal sinewaves was to investigate the time-dependent transfer of heat and moisture when the wall specimens were comparatively moist. During the final summer period, the accumulated moisture migrated towards the interior surface thereby drying the exterior layers of construction.

## Measurements

Each wall specimen was instrumented with sensors for the measurement of temperature, heat flux and moisture content. Sensor locations are shown in Figure 6 for a typical wall construction having a layer of exterior sheathing.

### *Temperature*

Surface and air temperatures were measured with copper-constantan (type-T), bead thermocouples. The thermocouples were fabricated from 30 gauge duplex wire (0.25 mm diameter). The thermocouple wire was calibrated by NIST's Thermometry Group (Semerjian 1991) in accordance with the International Temperature Scale of 1990 (ITS-90).

### *Heat flux*

The rate of heat flux through the meter section of each wall specimen was measured with a single heat-flux transducer. As shown in Figure 6, the transducer was placed at the geometric center of the interior surface of the gypsum wallboard for specimens 1 through 9 and 12. For specimens 10 and 11, however, the transducer was located at the same height but 30 mm off-center from the air-leakage holes described above. The heat flux transducers were attached to the gypsum wallboard with a silicone-rubber adhesive. The transducers on wall specimens 3, 4, and 9 to 12 were painted with white latex paint.

The heat flux transducers consisted of a small disk of silicone rubber, 23 mm in diameter and 3 mm thick, containing a series of thermocouple junctions (e.g., thermopile) embedded on opposite faces of the sensor. The junctions were wound in a helical spiral within a sensing region about 20 mm in diameter. The thermopile generated an emf directly proportional to the temperature difference across the sensing region, which was, for practical purposes, proportional to the heat flux through the transducer.

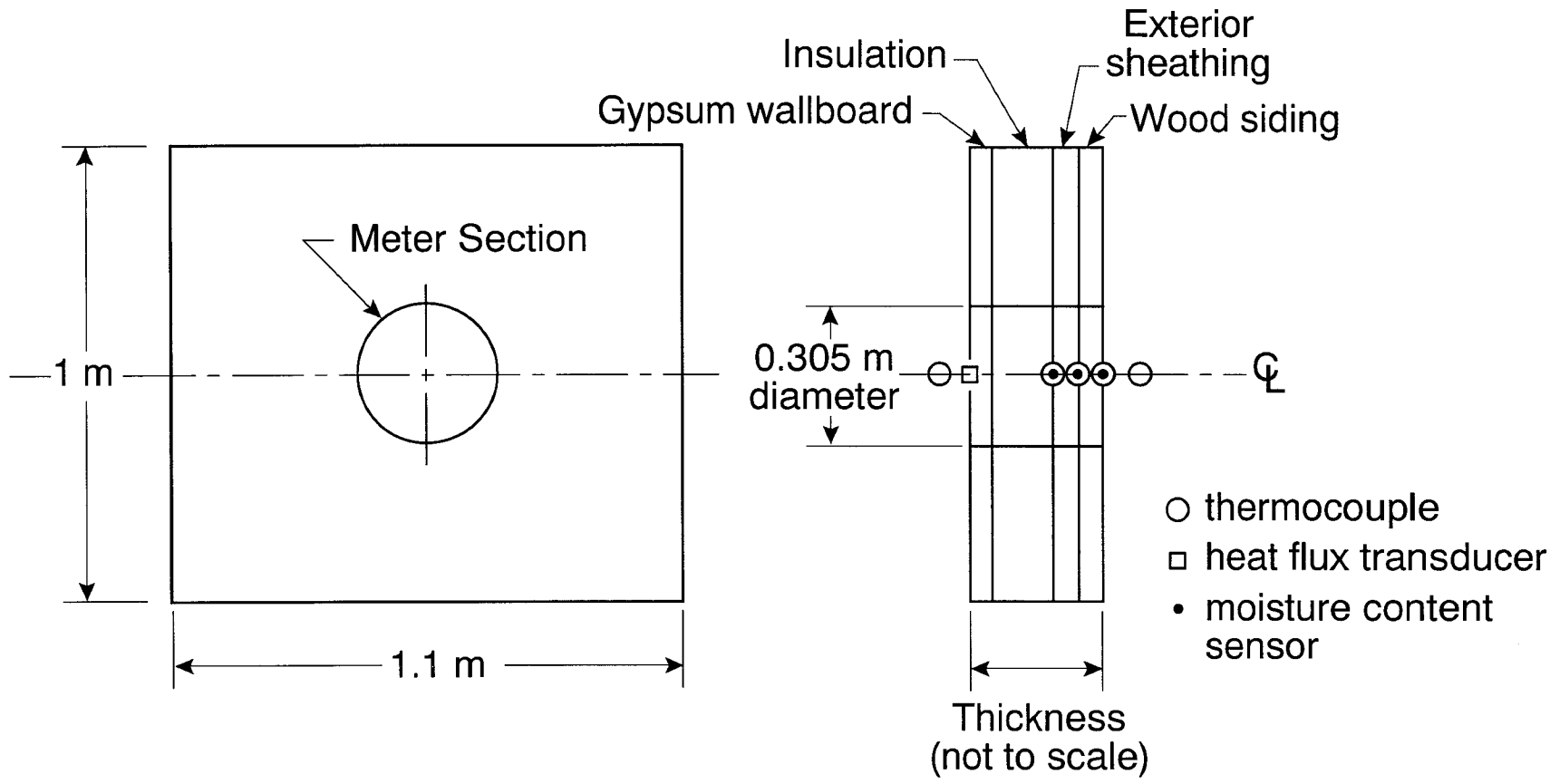
WALL SPECIMEN SENSOR LOCATIONS
Insulation
Exterior sheathing
Gypsum wallboard
Wood siding
Meter Section
1 m
0.305 m diameter
1.1 m
Thickness (not to scale)
thermocouple
heat flux transducer
moisture content sensor

Figure 6

The heat flux transducers were calibrated by placing them between an assembly of thermal insulation and subjecting them to a steady heat flux in NIST's 1-m guarded hot plate (Rennex 1983). The assembly consisted of a 25-mm thick glass-fiber board, a layer of 3-mm thick silicone rubber, and a second 25-mm thick glass-fiber board. Twelve circular openings were cut in the layer of silicone rubber to accommodate the transducers. In order to simulate test conditions within the calibrated hot box, the transducers were initially calibrated at a mean temperature of 21 °C and temperature differences of 5, 10, 20, and 30 °C, providing heat fluxes from approximately 3 $W/m^2$ to 18 $W/m^2$. The test conditions were repeated with the orientation of the transducers inverted to study the effect of heat reversal through the transducer.

After obtaining a steady-state heat flux, data were collected at 5 minute intervals over a one-hour period. The data were fit to an equation of the form:

$$q = A_0 + A_1 V \ . \tag{1}$$

A typical curve-fit is shown in Figure 7. The functional form of eq (1) was selected to account for the small (artificial) offset when the heat flux was zero. A summary of the regression curve-fits for the heat flux transducers and the residual standard deviation for the fit is provided in Table 3.

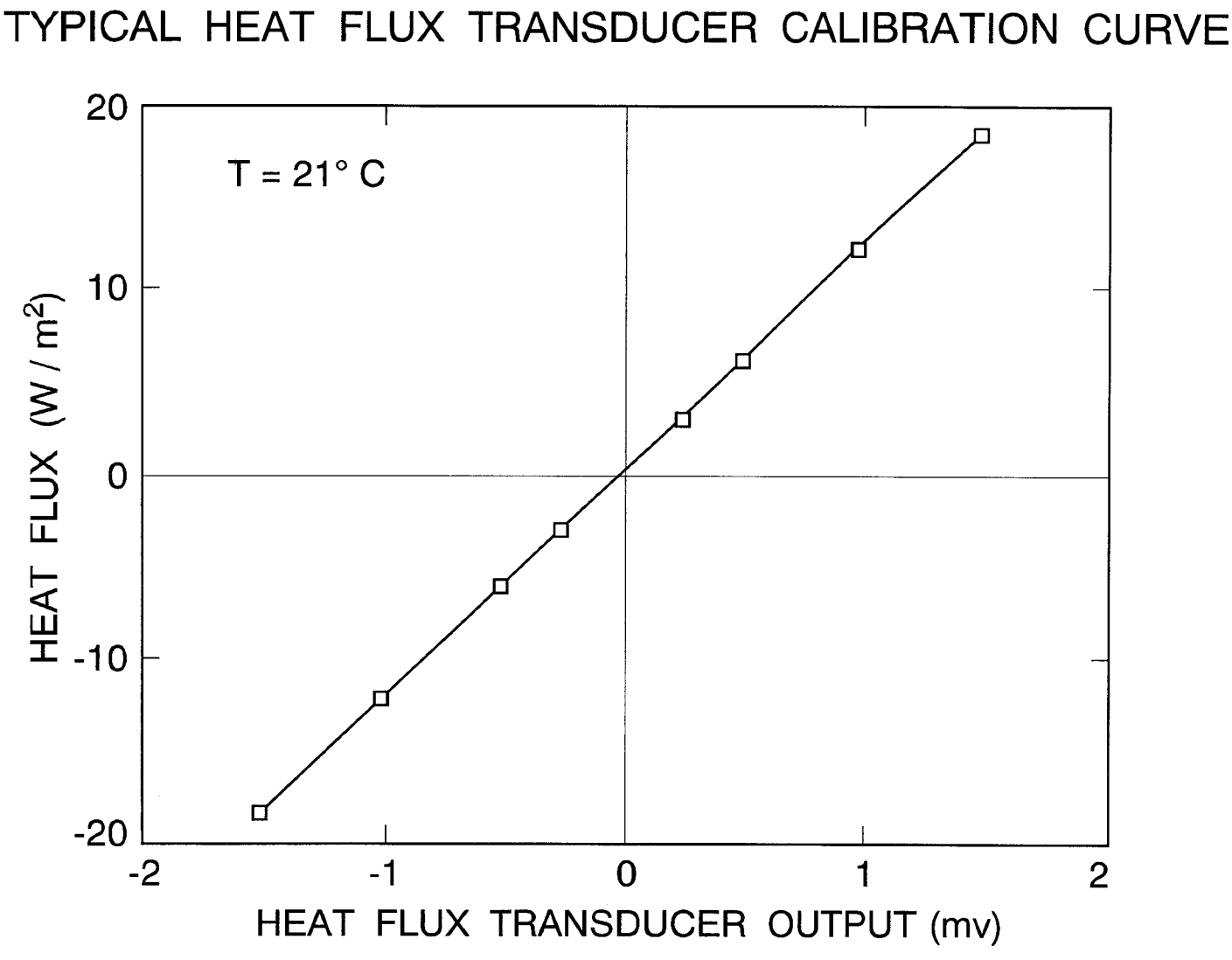
TYPICAL HEAT FLUX TRANSDUCER CALIBRATION CURVE
T = 21° C
HEAT FLUX (W / m2)
20
10
0
-10
-20
-2
-1
0
1
2
HEAT FLUX TRANSDUCER OUTPUT (mv)

Figure 7

| Table 3<br>Heat Flux Transducer Regression Coefficients | | | |
|---|---|---|---|
| Transducer | $A_0$ ($W/m^2$) | $A_1$ ($W/m^2 \cdot mV$) | Residual Standard Deviation of Fit ($W/m^2$) |
| 1 | 0.114 | 11.967 | 0.021 |
| 2 | 0.169 | 12.411 | 0.042 |
| 3 | 0.159 | 12.154 | 0.034 |
| 4 | 0.146 | 12.389 | 0.031 |
| 5 | 0.102 | 12.147 | 0.030 |
| 6 | 0.175 | 12.239 | 0.048 |
| 7 | 0.102 | 11.244 | 0.024 |
| 8 | 0.093 | 10.983 | 0.026 |
| 9 | 0.062 | 11.226 | 0.045 |
| 10 | 0.195 | 10.805 | 0.068 |
| 11 | 0.156 | 10.502 | 0.044 |
| 12 | 0.160 | 11.547 | 0.039 |

*Moisture Content*

The moisture content of the wood-based materials was measured using the electrical-resistance method (Duff 1968). This method is based on the principle that, below fiber-saturation, there exists a unique relationship between moisture content and electrical resistance for a particular species of wood. For this experiment, a commercial moisture meter based on this principle and having a display resolution of 0.1 percent moisture content was adapted in the following manner. The two-pin metal electrodes provided with the moisture meter were replaced with a pair of electrodes comprised of electrically conductive epoxy. The epoxy was applied to the surface of the wood-based materials in strips normal to the grain as illustrated in Figure 8a. The sensors were fabricated by mixing together equal parts of a two-component silver epoxy. Using a template, the mixture was applied to the surface of the material as two strips, each approximately 4 mm wide with a centerline to centerline spacing of 23 mm. Before curing, bare-wire leads were placed in the mixture (one lead per strip). The mixture was allowed to cure at room temperature for a minimum of 24 hours.

# CONSTRUCTION AND LOCATION OF MOISTURE CONTENT SENSORS

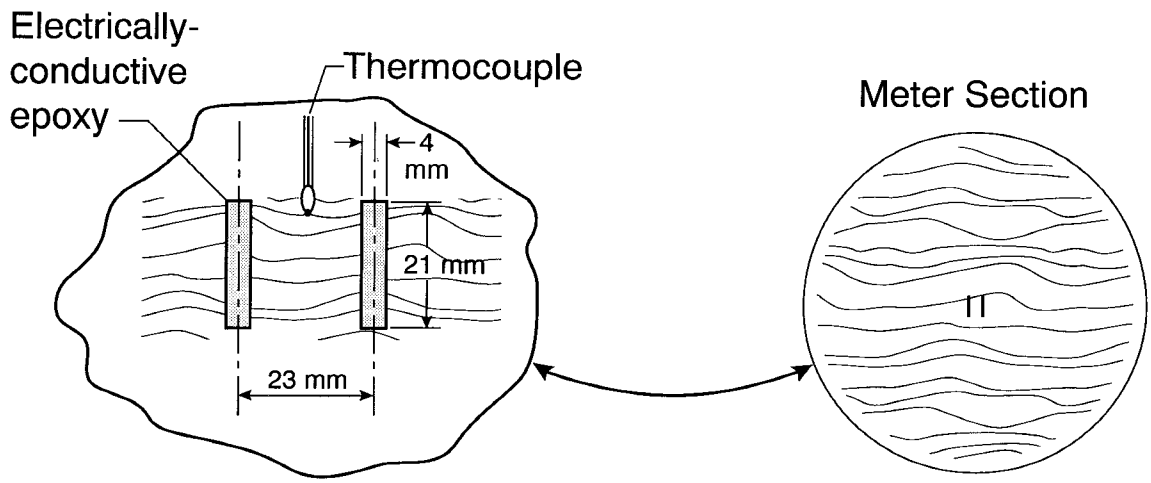


(a) Moisture content sensor normal to direction of wood grain

(b) General configuration

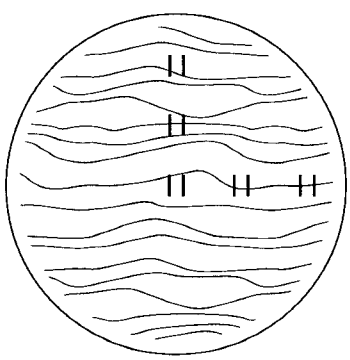

(c) Wall 1 configuration
Interior surface of sugar pine

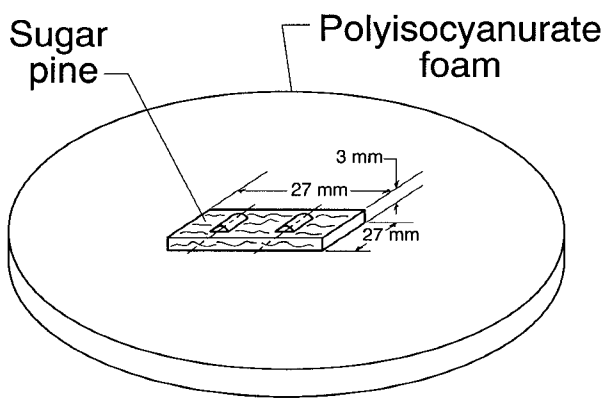


(d) Moisture content sensor on sugar pine substrate

Figure 8

Moisture content sensors were applied to the interior and exterior surfaces of the sugar pine and to the interior surfaces of the plywood and fiberboard. With the exception of the interior surface of the sugar pine sheathing of wall specimen 1, the sensors were located at the geometric center of each wall specimen as illustrated in Figures 6 and 8b. A special array of five sensors was applied to the interior surface of the sugar pine of wall specimen 1 to investigate the lateral distribution of moisture (fig. 8c). For wall specimens 9 to 12, a substrate of sugar pine with epoxy electrodes was attached to the foil-faced polyisocyanurate sheathing with a silicone rubber (fig. 8d).

At the completion of the calibrated hot box experiment, all 24 of the moisture content sensors were calibrated collectively in a small environmental chamber. Since the sensors had been attached permanently to the wood-based materials, a 100 by 100 mm section of material (with the attached sensor) was cut from the wall specimen and placed in a two-pressure humidity generator (Hasegawa and Little 1977). The sensors were exposed to fixed relative humidities of 50, 65, 80 and 92 percent at 4.4 °C, and 50, 65, 80, 90 and 95 percent at 32.2 °C. Readings were taken from each sensor at daily intervals using the commercial moisture meter. The meter readings for one sensor attached to sugar pine are plotted versus elapsed time in Figure 9. Note that at 65 percent relative humidity and 4.4 °C, it required nearly 50 days for the sugar pine substrate to obtain moisture equilibrium.

The calibration for each sensor was determined by comparing the equilibrium moisture-meter readings to the actual moisture content of the wood-based substrate material. The calibration data for one sensor attached to sugar pine is given in Figure 10. Here, the actual moisture content of the wood-based material was determined from a previously established relationship between moisture content and relative humidity, known as the sorption isotherm.[1] Linear regression curves were fit to the data at 4.4 °C and 32.2 °C for each sensor. The calibration curves were subsequently used to correct the data collected from wall specimens during the calibrated hot box experiment. The moisture content at temperatures between 4.4 °C and 32.2 °C was determined by linear interpolation.

The analysis of the calibration data revealed considerable variability between the sensors attached to sugar pine. An example is given in Figure 11 for data from 23 moisture content sensors conditioned at 4.4 °C. Note that the variability between sensors increased at higher moisture contents. The data point for the sensor in contact with cellulose was excluded from the graph since the presence of fire retardants in the cellulose caused the sensor to give erroneous readings (Laurenzi 1994). The variability in the data for the 23 sensors was further examined by plotting the meter readings at 32.2 °C and 95 percent relative humidity versus the sensor number as illustrated in Figure 12. The middle line corresponds to the mean of the data and the dashed lines are one standard deviation from the mean. The standard deviations for the sugar pine

---

[1]During the calibration tests, the sensors and substrates were exposed to a sequence of increasing relative humidity conditions, so the "adsorption" isotherm, as opposed to the "desorption" isotherm, was used.

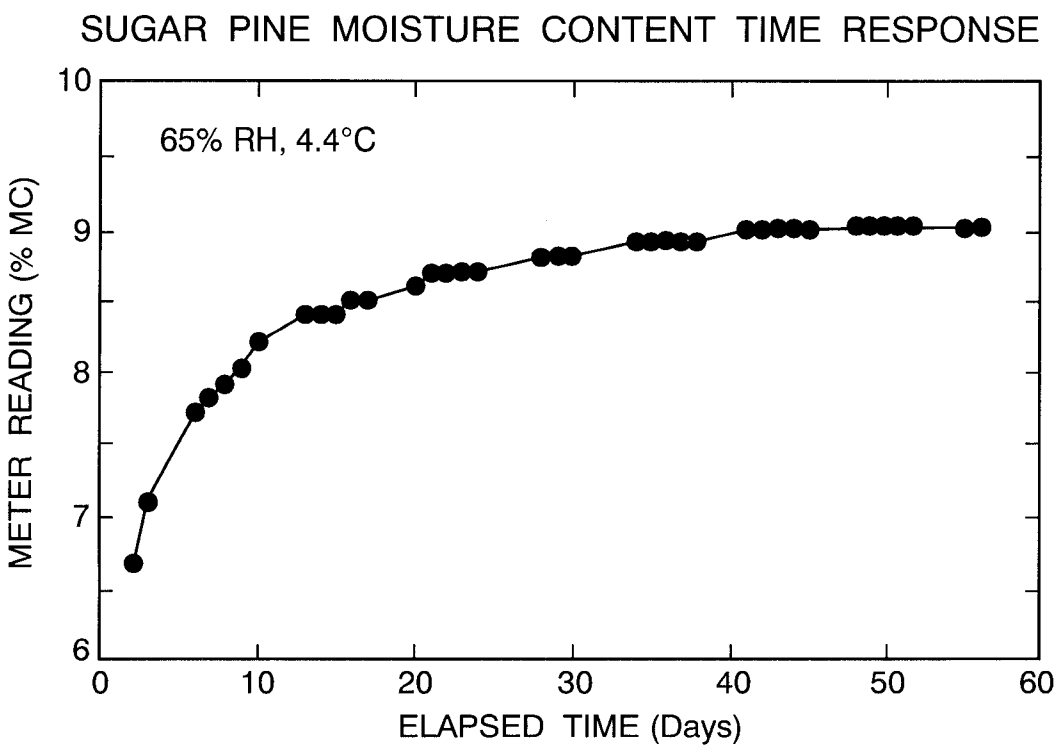


Figure 9

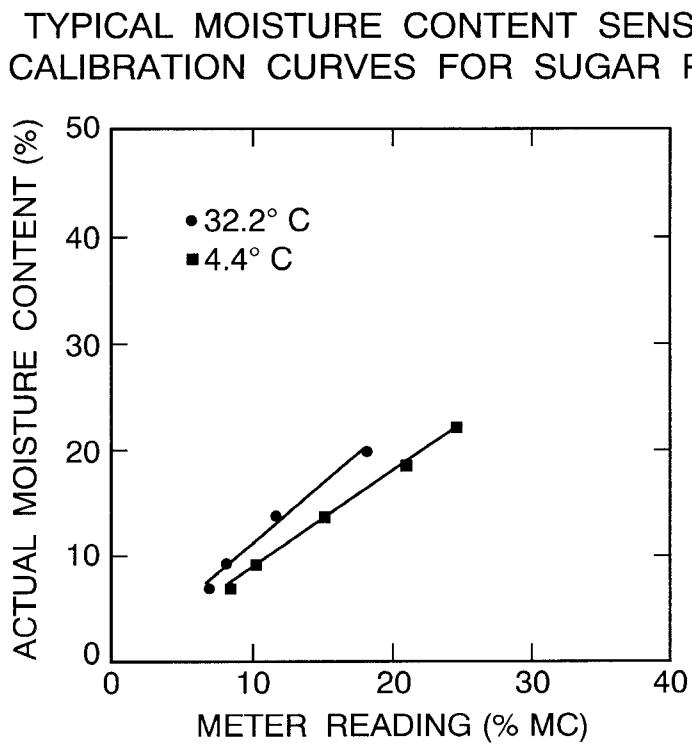


Figure 10

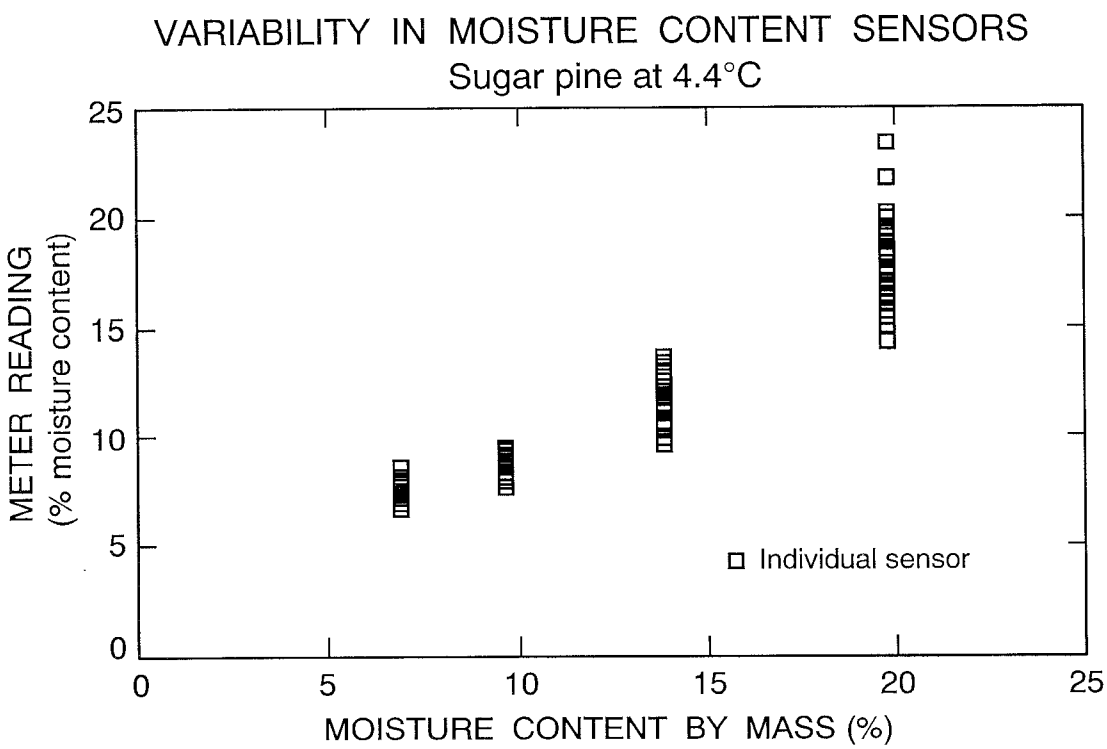


Figure 11

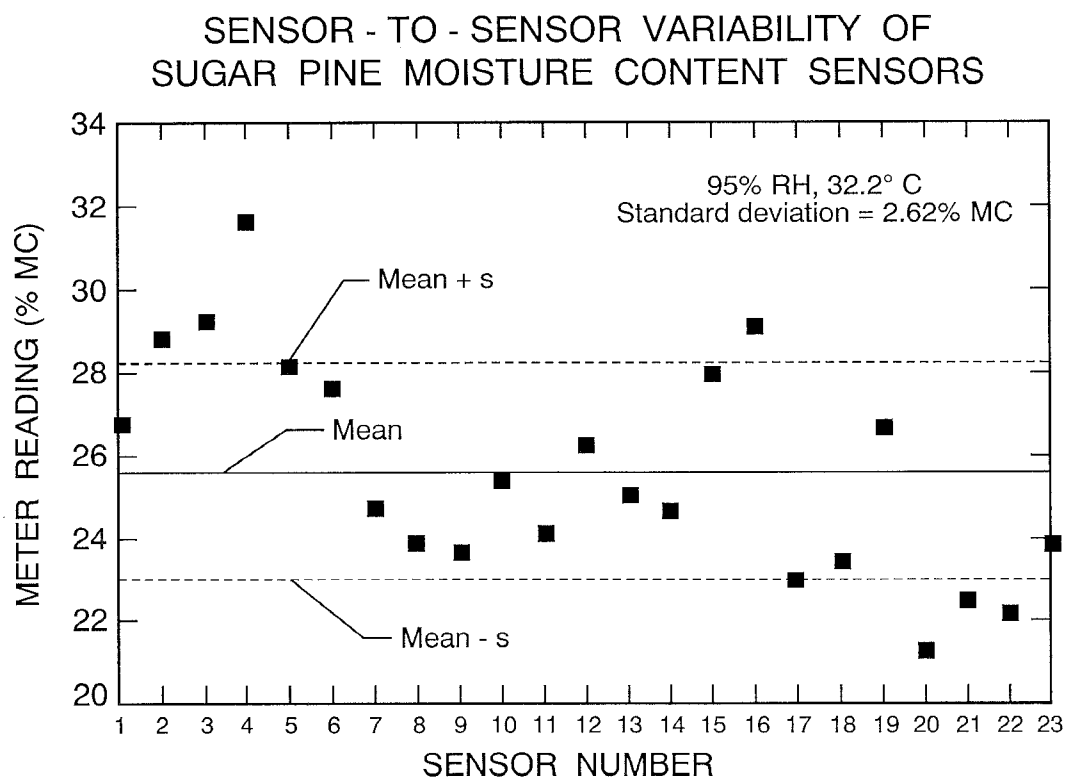


Figure 12

moisture content sensors at the other calibration conditions are given in Table 4. The results indicate that significant errors, particularly at high relative humidities, would result if a single calibration were used to represent all the sugar pine substrates.

**Table 4**
**Standard Deviation of Sugar Pine Moisture Content Sensors (%MC)**

| Relative Humidity (%) | Ambient Temperature 4.4 °C | 32.2 °C |
|---|---|---|
| 50 | 0.43 | 0.39 |
| 65 | 0.48 | 0.66 |
| 80 | 1.13 | 0.85 |
| 90 | -- | 1.80 |
| 92 | 2.21 | -- |
| 95 | -- | 2.62 |

***Relative Humidity***

The relative humidities of the metering and climatic chambers were measured using commercial thin-film capacitance humidity sensors. The sensors were calibrated using a chilled-mirror dew point hygrometer and a precision dry-bulb thermometer. The relative-humidity sensor for the metering chamber was calibrated at 21 °C from 30 to 70 percent relative humidity whereas, the climatic chamber sensor was calibrated from 20 to 80 percent relative humidity at various temperatures, Figure 13.

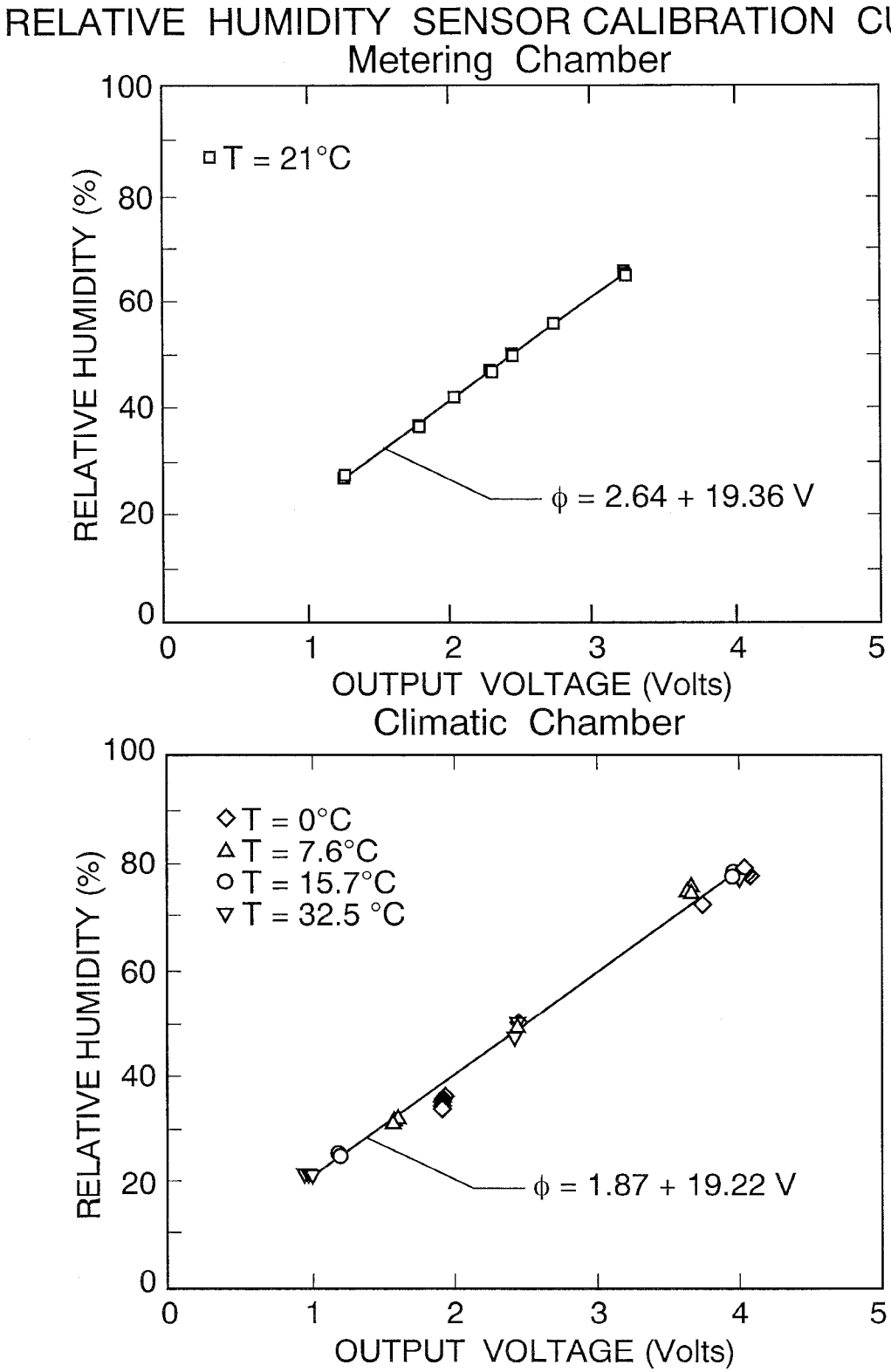
RELATIVE HUMIDITY SENSOR CALIBRATION CURVES
Metering Chamber
T = 21°C
ϕ = 2.64 + 19.36 V
RELATIVE HUMIDITY (%)
OUTPUT VOLTAGE (Volts)
Climatic Chamber
T = 0°C
T = 7.6°C
T = 15.7°C
T = 32.5 °C
ϕ = 1.87 + 19.22 V
RELATIVE HUMIDITY (%)
OUTPUT VOLTAGE (Volts)

Figure 13

# SPECIMEN MATERIALS PROPERTIES

MOIST requires that moisture and heat transfer properties for each material layer within a wall specimen be provided as input data. Currently, the program has a database of "representative" properties for 28 building materials commonly used in residential construction. In order to minimize the uncertainties associated with material variability, the following properties - sorption isotherm, permeability, and thermal conductivity - were measured for each of the materials used in the wall specimens. The experimental procedures and resulting data for these properties are summarized in this section.

## Sorption Isotherms

The sorption isotherms were determined by placing eight small specimens of each hygroscopic material in vessels above saturated salt-in-water solutions. For a given temperature, each saturated salt-in-water solution provided a fixed relative humidity (Greenspan 1977). In this case, the vessels were maintained at a temperature of 24 $\pm$ 0.2 °C until the specimens reached steady-state equilibrium. The equilibrium moisture content was plotted versus relative humidity to give the sorption isotherm. Separate sorption isotherm data were obtained for specimens initially dry (adsorption isotherm) and for specimens initially saturated (desorption isotherm). A detailed description of this measurement method is given elsewhere (Richards et al. 1992). The mean of the absorption and desorption isotherm measurements was fit to an equation of the form:

$$\gamma = \frac{B_1 \phi}{(1+B_2\phi)(1-B_3\phi)} \quad . \tag{2}$$

The coefficients $B_1$, $B_2$, and $B_3$ were determined by regression analysis and are summarized in Table 5. The sorption isotherm data for sugar pine and corresponding curve-fit are illustrated in Figure 14.

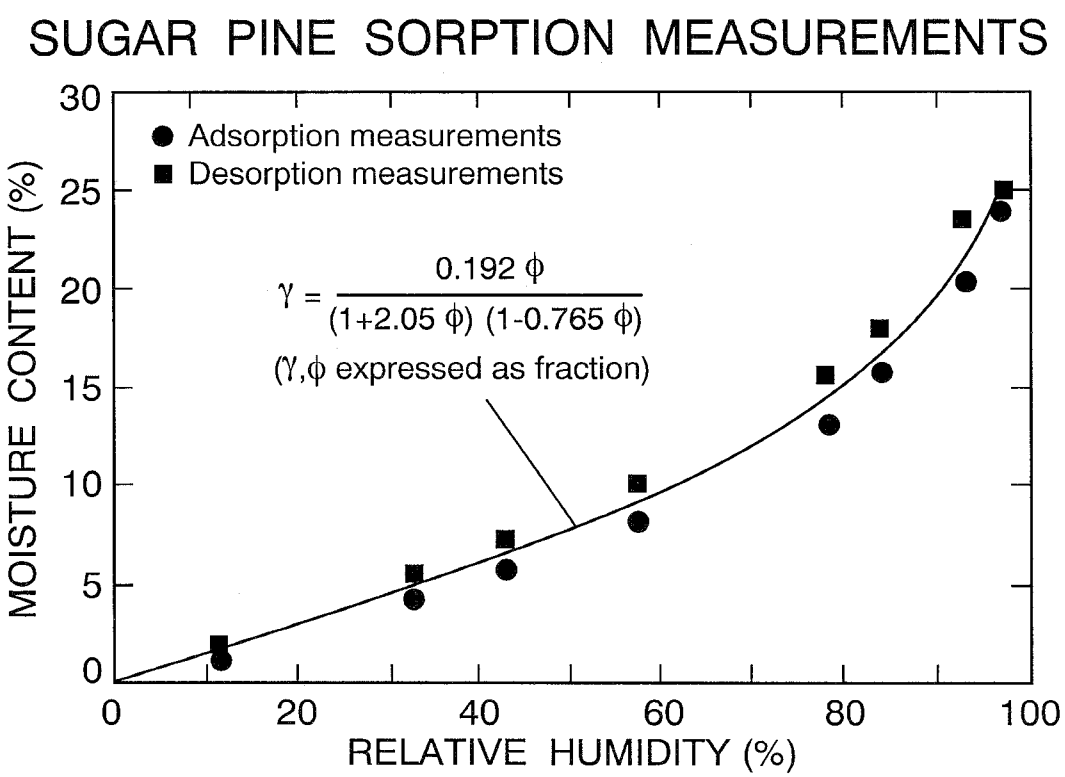
SUGAR PINE SORPTION MEASUREMENTS
Adsorption measurements
Desorption measurements
$\gamma = \frac{0.192\,\phi}{(1+2.05\,\phi)\,(1-0.765\,\phi)}$
($\gamma$,$\phi$ expressed as fraction)
MOISTURE CONTENT (%)
RELATIVE HUMIDITY (%)
0
5
10
15
20
25
30
0
20
40
60
80
100

Figure 14

| Table 5<br>Sorption Isotherm Regression Coefficients | | | |
|---|---|---|---|
| **Materials** | **$B_1$** | **$B_2$** | **$B_3$** |
| Cellulose loose fill | 0.274 | 5.95 | 0.9995 |
| Fiberboard sheathing | 1.14 | 50.6 | 0.923 |
| Polyisocyanurate foam | 0.0528 | 2.51 | 0.773 |
| Glass-fiber insulation | 0.00170 | $1 \times 10^{-8}$ | 0.963 |
| Gypsum wallboard | 0.00336 | $1 \times 10^{-8}$ | 0.901 |
| Kraft paper with asphalt mastic | 51.9 | 2538 | 0.902 |
| Plywood sheathing (fir) | 0.488 | 8.93 | 0.804 |
| Sugar pine | 0.192 | 2.05 | 0.765 |

## Permeability Measurements

The water vapor permeability of the rigid hygroscopic materials was determined using permeability cups placed in controlled environments. Five circular specimens, 140 mm in diameter, of each material were sealed at the top of open mouth glass dishes. The dishes were subsequently placed and sealed inside glass vessels maintained at a fixed temperature. Saturated salt-in-water solutions were used inside the glass dish and surrounding glass vessels to generate a relative humidity difference of approximately 10 percent across each specimen. By using different salt solutions, the mean relative humidity across the specimen ranged from "dry" to a nearly saturated state. A detailed description of the permeability measurement method is given elsewhere (Burch et al. 1992).

Permeability data were plotted versus the mean relative humidity across the specimen and fit to an equation of the form:

$$\mu = \exp(C_1 + C_2\phi + C_3\phi^2) \ . \qquad (3)$$

The coefficients $C_1$, $C_2$, and $C_3$ were determined by regression analysis and are summarized in Table 6.

| Table 6<br>Permeability Regression Coefficients | | | |
|---|---|---|---|
| **Materials** | **$C_1$** | **$C_2$** | **$C_3$** |
| Cellulose loose fill[1] | −22.425 | 0.0 | 0.0 |
| Fiberboard sheathing | −24.054 | −.1004 | 0.0 |
| Polyisocyanurate foam | −26.686 | 0.5224 | 0.0 |
| Glass-fiber insulation[1] | −22.425 | 0.0 | 0.0 |
| Gypsum wallboard | −23.475 | 0.0 | 0.0 |
| Kraft paper with asphalt mastic | −32.239 | −1.168 | 3.058 |
| Plywood sheathing (fir) | −25.534[2] | −0.9178[2] | 0.8858[2] |
| Sugar pine | −28.677 | −0.9198 | 4.576 |

[1]Assumed to be equal to stagnant air layer.
[2]These coefficients were fit to the equation: $\mu = \exp [C_1 + C_2\phi (1 - C_3\phi)]$

The permeability of one material, sugar pine, is illustrated in Figure 15. As noted in Figure 15 and previous data (Burch et al. 1992), measurements conducted at 7 °C and 24 °C revealed that, for the given range, temperature has only a small effect on permeability.

Special water vapor transmission measurements (Appendix B) were conducted to determine the permeance of the paint layers applied to interior and exterior surfaces of the wall specimens. The Lewis relationship between heat and mass transfer (Threlkeld 1970) was used to calculate the vapor permeance of the cavity airspace for wall specimen 7. The permeance of the paint layers and the cavity airspace are given in Table 7.

| Table 7<br>Permeance of Paint Layers and Convective Airspace | |
|---|---|
| **Layers** | **Permeance ($10^{-12}$kg/s·m²·Pa)** |
| Interior latex paint | 977 |
| Exterior latex paint | 190 |
| Exterior oil-base paint | 80.4 |
| Cavity airspace | 13,300 |

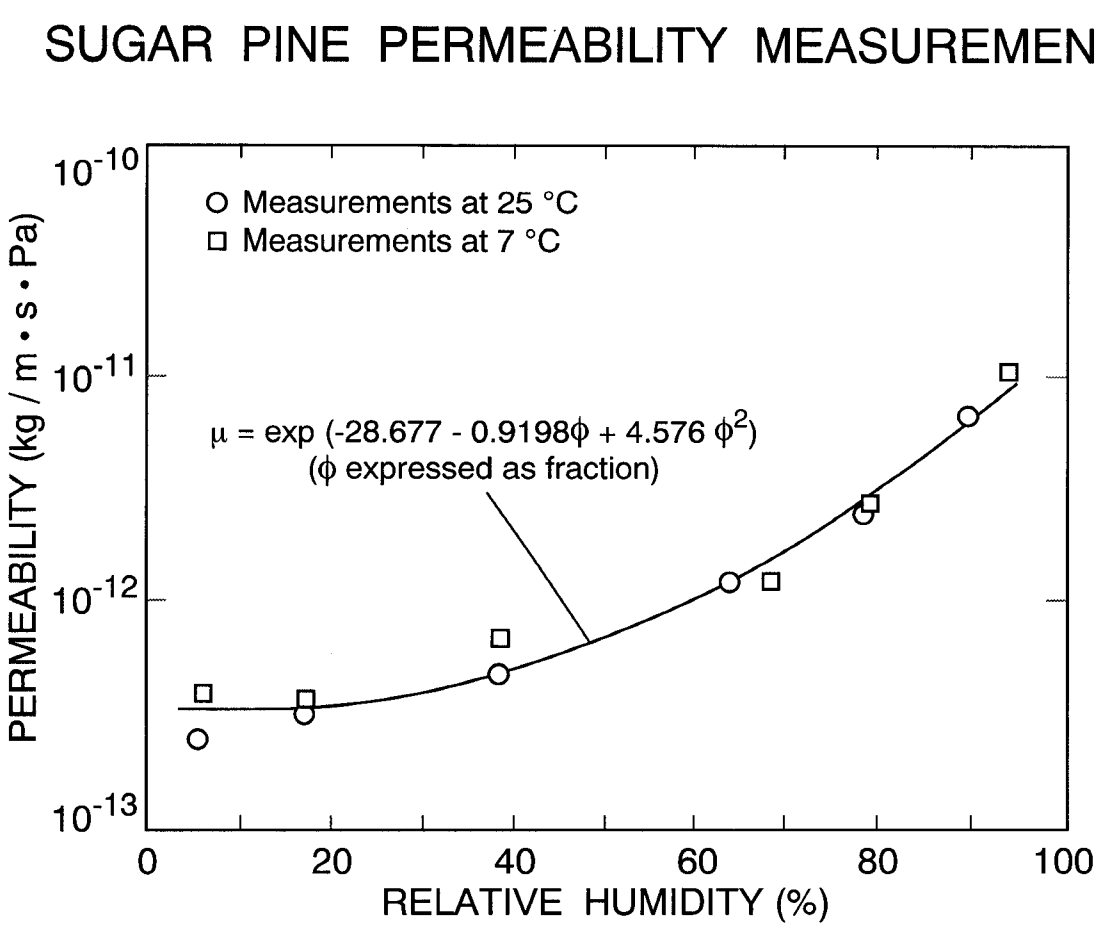
SUGAR PINE PERMEABILITY MEASUREMENTS
PERMEABILITY (kg / m • s • Pa)
10-10
10-11
10-12
10-13
Measurements at 25 °C
Measurements at 7 °C
μ = exp (-28.677 - 0.9198ϕ + 4.576 ϕ2)
(ϕ expressed as fraction)
0
20
40
60
80
100
RELATIVE HUMIDITY (%)

Figure 15

## Thermal Conductivity Measurements

The thermal conductivities of the wall specimens were determined using NIST's one-meter guarded hot plate apparatus, ASTM Test Method C 177 (ASTM 1994). The apparatus is designed to determine the steady-state thermal transmission properties of flat specimens of building materials. A schematic diagram of the operating principle for the apparatus is illustrated in Figure 16. In practice, the apparatus produces a one-dimensional heat flow normal to the meter area of the guarded hot plate. Under steady-state conditions, the thermal conductivity of the specimen was determined from Fourier's equation for one-dimensional heat flow, namely:

$$Q = \lambda A \frac{\Delta T}{L} . \qquad (4)$$

Specimens of cellulose and rigid materials were prepared from the surplus materials used to construct the wall specimens. The cellulose specimen was prepared by first lofting and then hand-pouring the insulation into a fine wire-mesh basket. The wire mesh was subsequently neglected in the thermal conductivity measurement. The amount of cellulose was determined to provide the same nominal density as that installed in the wall specimen. The specimens of glass-fiber thermal insulation were taken carefully from each wall specimen at the conclusion of the calibrated hot box experiment and measured individually. The specimens were preconditioned at 21 $\pm$ 2 °C and 40 to 60 percent relative humidity for about 2 months prior to the guarded hot plate tests.

The thermal conductivity of each specimen was measured at nearly the same mean temperature that the material experienced during the steady-state winter exposure in the calibrated hot box experiment. Consequently, the thermal conductivity of gypsum wallboard was determined at a mean temperature of 20.5 °C; the thermal insulations in the wall cavity, at 15 °C; the exterior sheathing, at 8.5 °C; and the exterior siding, at 7.5 °C. The specimens of cellulose and glass-fiber thermal insulation were tested at the same thickness as the wall cavity, 81.4 mm. A temperature difference of 20 °C was selected for these materials and a value of 10 °C for the other specimens. The densities of the cellulose and glass-fiber specimens were determined for a 406-mm-diameter section corresponding to the meter area of the guarded hot plate. The results of the guarded hot plate tests are summarized in Table 8.

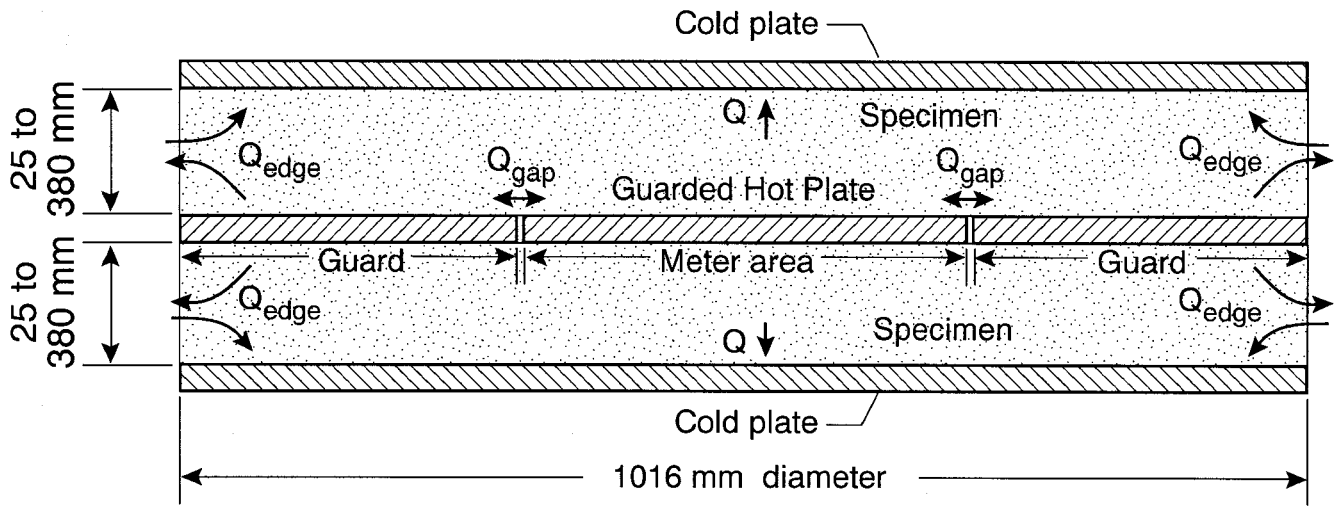
GUARDED HOT PLATE APPARATUS
Cold plate
25 to 380 mm
Q
Specimen
Q_edge
Q_gap
Guarded Hot Plate
Q_gap
Q_edge
Guard
Meter area
Guard
25 to 380 mm
Q_edge
Q_edge
Q
Specimen
Cold plate
1016 mm diameter

Figure 16

| Table 8<br>Guarded Hot Plate Measurements | | | | | | | |
|---|---|---|---|---|---|---|---|
| **Materials** | **Vapor Retarder** | **Specimen** | **Mean Temperature (°C)** | **Temperature Difference (°C)** | **Thickness (mm)** | **Density ($kg/m^3$)** | **Thermal Conductivity (W/m·K)** |
| Cellulose loose-fill | - | typical | 14.9 | 20.1 | 81.4 | 56 | 0.0397 |
| Fiberboard | - | typical | 8.5 | 10.0 | 13.2 | 380 | 0.0539 |
| Foil-faced polyisocyanurate | - | typical | 8.5 | 10.0 | 12.7 | 42 | 0.0210 |
| Glass-fiber insulation | No | 01 | 15.0 | 20.0 | 81.4 | 9.6 | 0.0433 |
| Glass-fiber insulation | No | 03 | 15.0 | 20.0 | 81.4 | 9.3 | 0.0436 |
| Glass-fiber insulation | No | 04 | 15.0 | 20.0 | 81.4 | 8.0 | 0.0466 |
| Glass-fiber insulation | No | 05 | 15.0 | 20.0 | 81.4 | 9.5 | 0.0434 |
| Glass-fiber insulation | No | 06 | 15.0 | 20.0 | 81.4 | 8.7 | 0.0455 |
| Glass-fiber insulation | No | 12 | 15.0 | 20.0 | 81.4 | 9.7 | 0.0443 |
| Glass-fiber insulation | Yes | 02 | 15.0 | 20.0 | 81.4 | 10.4 | 0.0422 |
| Glass-fiber insulation | Yes | 09 | 15.0 | 20.0 | 81.4 | 10.6 | 0.0435 |
| Glass-fiber insulation | Yes | 10 | 15.0 | 20.0 | 81.4 | 10.7 | 0.0421 |
| Glass-fiber insulation | Yes | 11 | 15.0 | 20.0 | 81.4 | 10.9 | 0.0417 |
| Gypsum wallboard | - | typical | 20.5 | 10.0 | 13.4 | 629 | 0.159 |
| Plywood | - | typical | 8.5 | 10.0 | 12.9 | 505 | 0.0752 |
| Sugar pine | - | typical | 7.5 | 10.0 | 18.2 | 374 | 0.0865 |

The thermal conductivities of the glass-fiber thermal insulation were plotted as a function of density as illustrated in Figure 17. Each point is individually identified by the specimen number and the type of symbol (square or diamond) indicated the presence of a vapor retarder. A regression curve of the form (Boulant et al. 1983)

$$\lambda = D_0 + D_1\rho + \frac{D_2}{\rho} \tag{5}$$

was fit to the data and is shown as a solid line in Figure 17. Values of $D_0$, $D_1$, and $D_2$ were determined to be 0.0121, $9.11 \times 10^{-4}$, and 0.219, respectively. This equation was subsequently used to compute values of thermal conductivity of the glass-fiber insulation at other densities.

After the guarded hot plate tests, core samples of the glass-fiber insulation were taken to determine the local in-situ density corresponding to the location of the heat flux transducer. Cylindrical core samples, having the same diameter as the heat flux transducers, were taken in-line with the heat flux transducers. Using eq (5), thermal conductivity values for the glass-fiber insulation were determined for the wall specimens and are summarized in Table 9. It should be noted that the densities obtained for the core samples for wall specimens 4 and 6 were below the range (8-11 $kg/m^3$) of the density/thermal-conductivity correlation.

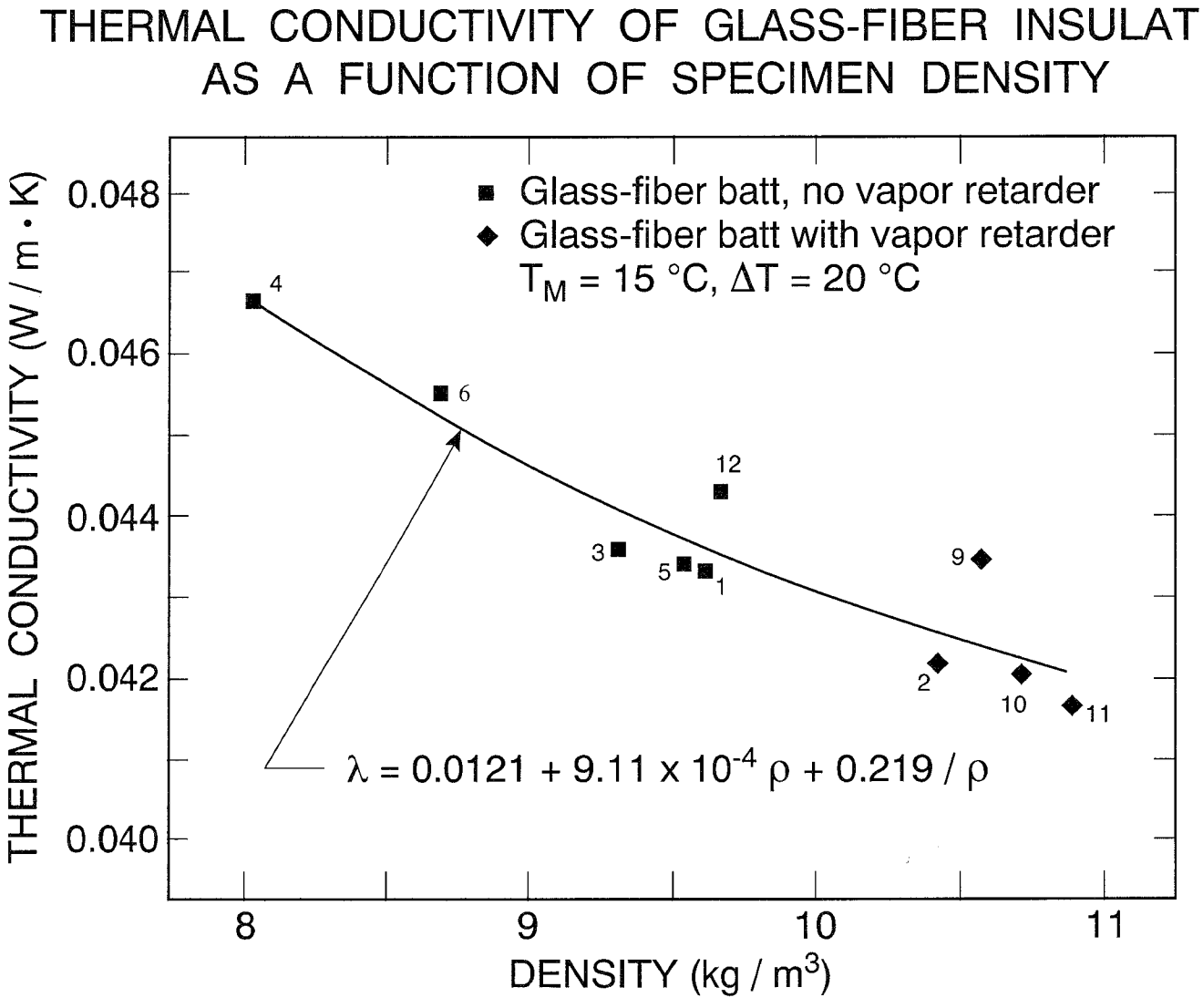
THERMAL CONDUCTIVITY OF GLASS-FIBER INSULATION
AS A FUNCTION OF SPECIMEN DENSITY
Glass-fiber batt, no vapor retarder
Glass-fiber batt with vapor retarder
$T_M$ = 15 °C, ΔT = 20 °C
$\lambda = 0.0121 + 9.11 \times 10^{-4} \rho + 0.219 / \rho$
THERMAL CONDUCTIVITY (W / m • K)
0.048
0.046
0.044
0.042
0.040
8
9
10
11
DENSITY (kg / m$^3$)
4
6
12
3
5
1
9
2
10
11

Figure 17

**Table 9**
**Local Thermal Conductivities for Cylindrical Core Samples of Glass-Fiber Batt Insulation**

| Wall Specimen | Density ($kg/m^3$) | Thermal Conductivity ($W/m \cdot K$) |
|---|---|---|
| 1 | 9.09 | 0.0445 |
| 2 | 9.17 | 0.0443 |
| 3 | 10.4 | 0.0426 |
| 4 | 5.98 | 0.0542 |
| 5 | 8.78 | 0.0450 |
| 6 | 6.16 | 0.0533 |
| 9 | 7.00 | 0.0468 |
| 10[1] | 10.7 | 0.0421 |
| 11[1] | 10.9 | 0.0417 |
| 12 | 9.51 | 0.0438 |

[1] The heat flux transducer for this wall specimen was installed off center and the in-situ density could not be ascertained. The thermal conductivity was determined for a bulk density corresponding to the 305-mm-diameter meter section of the wall specimen.

# COMPARISON OF EXPERIMENTAL RESULTS TO MOIST

At the completion of the calibrated hot box experiment, the measured moisture contents of selected material layers and the heat fluxes through the specimens were compared to predicted values from MOIST simulations. For the simulations, the experimental air temperature and relative humidity in the metering and climatic chambers were used as input boundary conditions. The material properties of the wall specimens were determined from measurements described in the previous section and input to the program. The thermal insulation in the wall cavity was modeled as a nonstorage layer. That is, the storage of heat and moisture within the insulation was neglected and constant values of permeance and thermal resistance for the insulation were specified in the program. The results of the comparisons are summarized in this section.

## Moisture Content Comparisons

In order to make meaningful comparisons between the experimental data and MOIST, it was vital to assess whether the moisture transfer through the circular meter section was one-dimensional. To investigate the one-dimensional transfer of moisture, an array of five moisture sensors was installed at the inside surface of the sugar pine (fig. 8c). The moisture contents of these five sensors are plotted versus time in Figure 18. The variability of the moisture content measurements ranged within $\pm$ 1.6 percent moisture content. Therefore, the results do not indicate significant departure from one-dimensional moisture transfer.

### *Base Case - Wall Specimen 1*

The moisture content at the inside surface of the sugar pine for wall specimen 1 is given in Figure 19. The measured and predicted values are indicated by the solid and dashed lines, respectively. At time zero, the exterior air temperature decreased from 21 °C to 7.2 °C (fig. 5) and water vapor from the interior air diffused into the wall construction accumulating in the sugar pine. The moisture content increased to 24 percent after 48 days. This peak value of moisture content was only 3 percent below the fiber saturation of 27 percent shown in Figure 14. After 48 days, the air temperature at the exterior surface of the wall was increased to 32 °C causing water vapor to migrate towards the inside environment. Consequently, the moisture content at the inside wood surface decreased rapidly. The moisture content fluctuations (fig. 18 and 19) were caused by the diurnal sinewaves in the exterior ambient temperature.

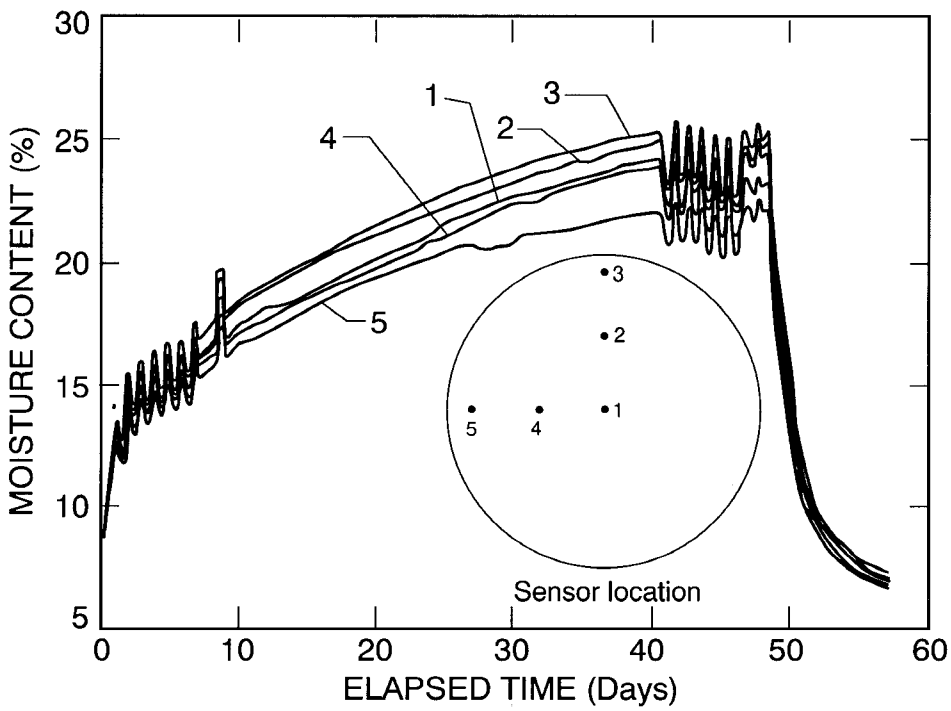


Figure 18

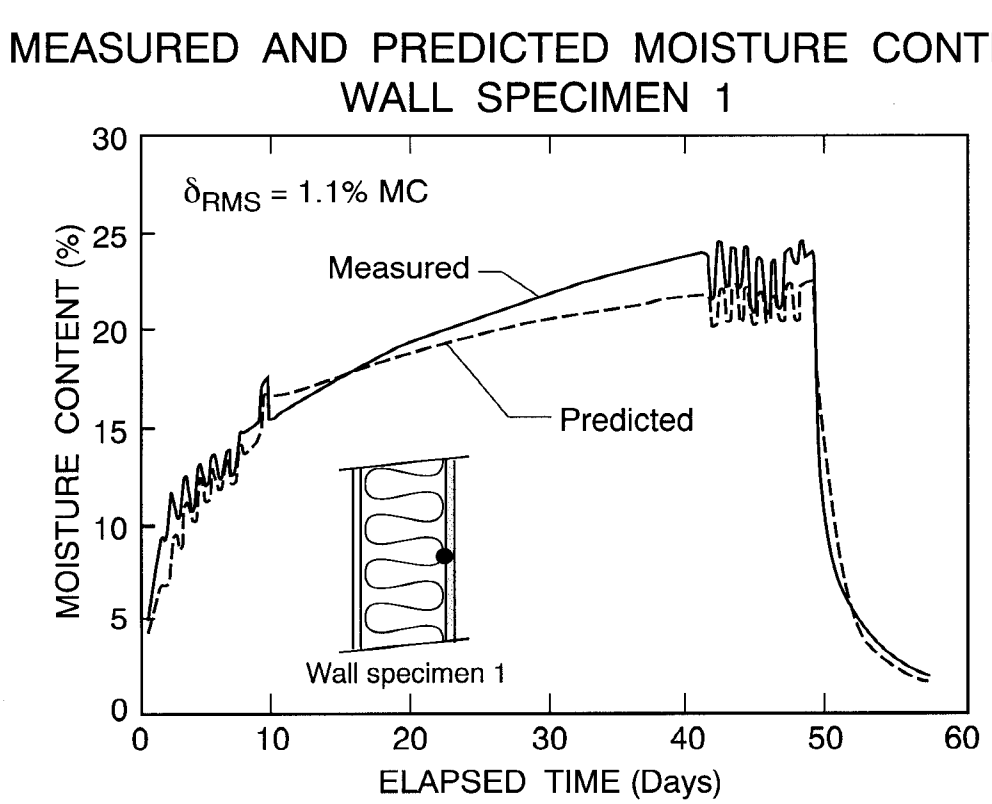


Figure 19

The predicted values of the moisture content (fig. 19) are for a 3.2-mm-thick layer of the inside surface of sugar pine. The average difference between the measured and predicted moisture content was expressed as a root-mean-square difference, or:

$$\delta_{RMS} = \sqrt{\frac{\sum_{n=1}^{N} (\Delta_n)^2}{N}} \quad . \tag{6}$$

As noted in Figure 19, the $\delta_{RMS}$ difference was 1.1 percent moisture content.

It was not possible to compare the measured and predicted moisture content at the outside surface of the sugar pine because the moisture content decreased below the minimum detectable limit (i.e., 6 percent) of the moisture meter. This drop in moisture content occurred because the outside wood surface was exposed to ambient air having a low relative humidity of 3 to 11 percent. The low relative humidity in the climatic chamber was necessary in order to minimize frost accumulation on the chamber's refrigeration coil. The authors acknowledge that such a low relative humidity is atypical of prevailing outdoor winter relative humidities.

### *Effect of Vapor Retarder - Wall Specimen 2*

A comparison of the measured and predicted moisture contents at the inside surface of the sugar pine for wall specimen 2 is given in Figure 20. The $\delta_{RMS}$ is 0.9 percent moisture content. Comparing Figures 19 and 20 indicates that the presence of the kraft-paper vapor retarder considerably reduced the water vapor diffusion into the wall construction, thereby significantly reducing the moisture content at the inside wood surface. In addition, the presence of the kraft-paper vapor retarder reduced the flow of moisture during the drying period, causing the moisture content at the inside wood surface to decrease at a slower rate.

### *Effect of Paint Coatings - Wall Specimens 3 and 4*

The results for wall specimen 3 with interior latex paint and exterior oil-base paint are given in Figure 21. Here the $\delta_{RMS}$ was 0.5 percent moisture content. The presence of the interior latex paint reduced the passage of water vapor into the wall construction, lowering the peak moisture content compared to wall specimen 1 (fig. 19).

Results for wall specimen 4 with interior and exterior latex paint are given in Figure 22. This wall is identical to wall specimen 3, except that exterior latex paint is used instead of exterior oil-base paint. Here the $\delta_{RMS}$ is 1.1 percent moisture content. Comparing Figures 21 and 22, very little difference in moisture content occurs as a result of using exterior latex paint instead of exterior oil-base paint. Moisture accumulation within the wood layer is caused by a difference between the inflow and outflow rates to the wood layer. A large difference in temperature and water vapor pressure across the gypsum wall board and the insulation layer causes a large inflow of moisture from the metering chamber to the wood layer. On the other

MEASURED AND PREDICTED MOISTURE CONTENT
WALL SPECIMEN 2

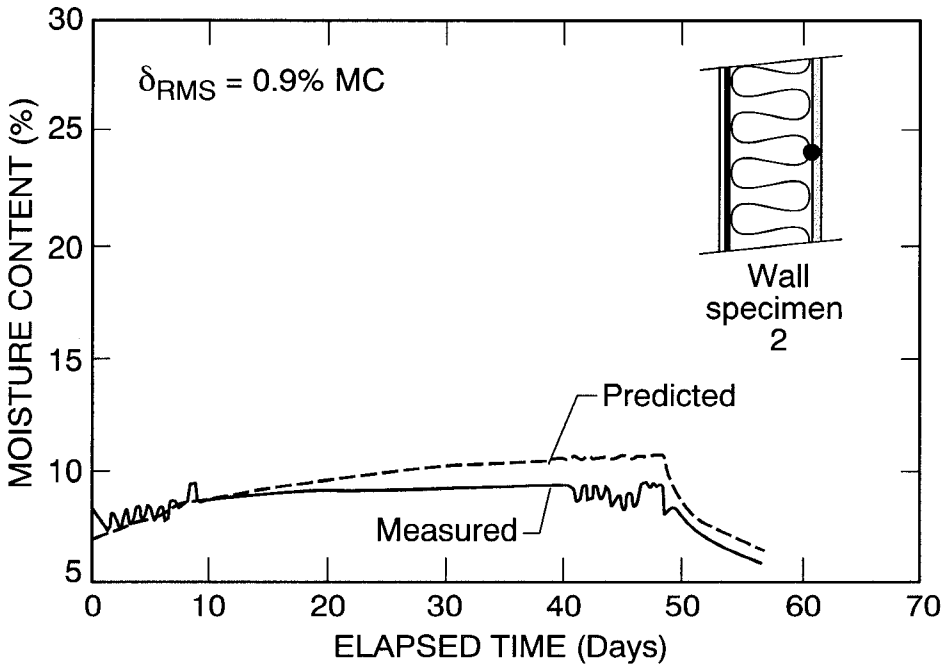


Figure 20

MEASURED AND PREDICTED MOISTURE CONTENT
WALL SPECIMEN 3

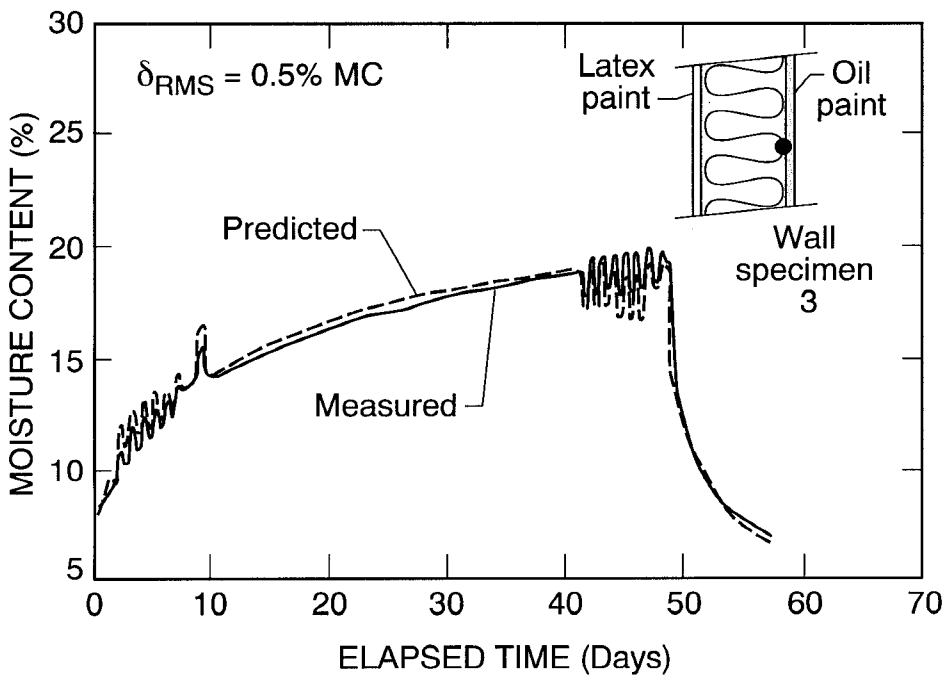


Figure 21

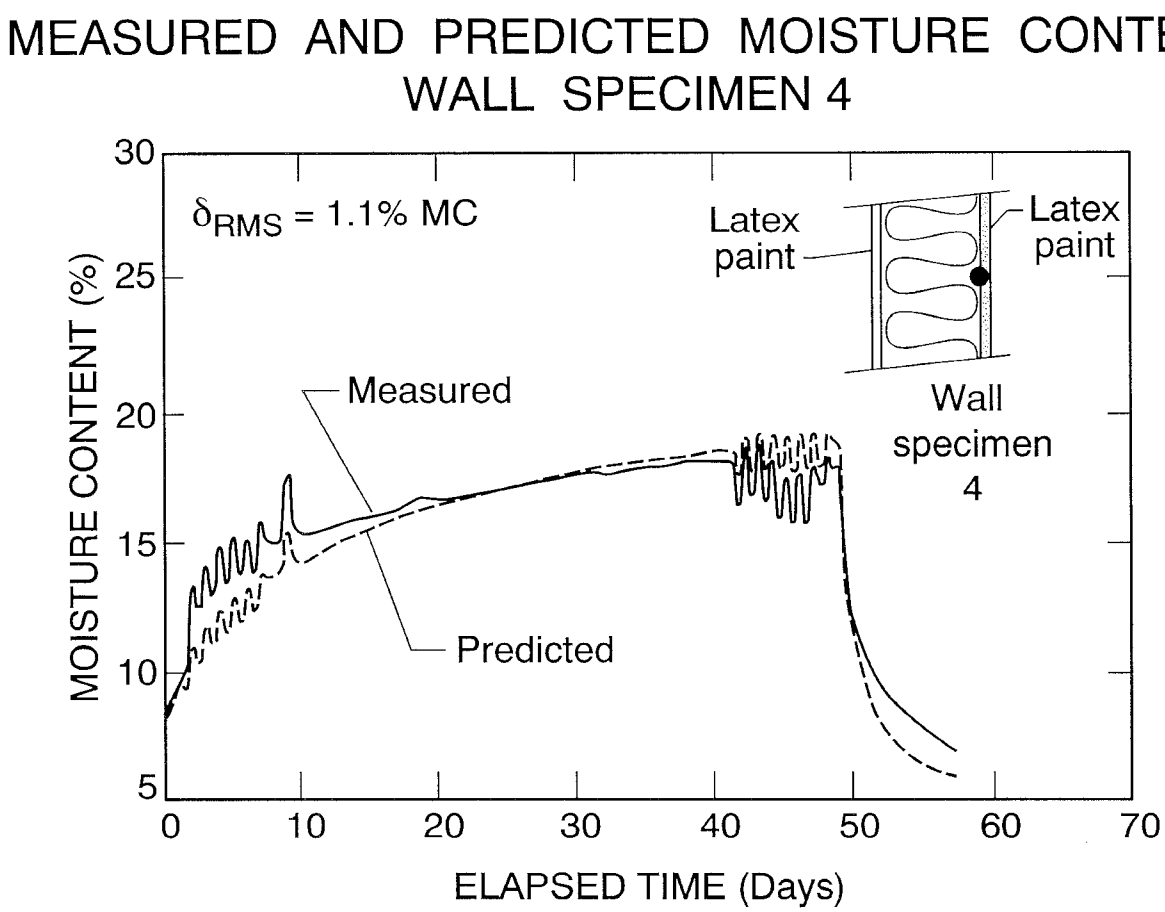
MEASURED AND PREDICTED MOISTURE CONTENT
WALL SPECIMEN 4
$\delta_{RMS}$ = 1.1% MC
Latex paint
Latex paint
Wall specimen 4
Measured
Predicted
MOISTURE CONTENT (%)
ELAPSED TIME (Days)
30
25
20
15
10
5
0
10
20
30
40
50
60
70

Figure 22

hand, a rather small difference in temperature and water vapor pressure exists across the wood layer. This causes the outflow of moisture to be relatively small in comparison with the inflow rate. The exterior paint permeance unquestionably affects the outflow of moisture. However, since the outflow rate is relatively small, the effect of exterior paint permeance on the rate of moisture accumulation within the wood layer is small.

*Effect of Sheathing - Wall Specimens 5 and 6*

A comparison between measured and predicted moisture content at the inside sheathing surface and the inside surface of the sugar pine for wall 5 is given in Figure 23. This wall is identical to wall specimen 1, except that fiberboard sheathing is installed between the insulation and the sugar pine. The $\delta_{RMS}$ is 0.8 percent moisture content at the inside surface of the fiberboard and 1.1 percent moisture content at the inside surface of the sugar pine, indicating good agreement between measured and predicted moisture contents. Comparing Figures 23 and 19, it is seen that the fiberboard sheathing provides additional moisture storage and reduces the peak moisture content at the inside wood surface.

A similar comparison for wall specimen 6 with plywood sheathing is given in Figure 24. Here the agreement between measured and predicted moisture contents is not as close. The $\delta_{RMS}$ between the measured and predicted is 1.5 percent moisture content at the inside plywood surface and 5.3 percent moisture content at the inside wood surface. The unsatisfactory prediction by MOIST for this wall specimen was attributed to the nonhomogeneity of the plywood, i.e., plywood is comprised of distinct layers of wood and glue. In the computer simulations, plywood was modeled as a homogeneous material.

*Effect of Cavity Insulation - Wall Specimens 7 and 8*

The results for wall specimen 7 are given in Figure 25. This wall is identical to wall specimen 1, except that thermal insulation was excluded leaving only an airspace in the wall cavity. The $\delta_{RMS}$ of 0.6 indicates good agreement between the measured and predicted moisture contents. Comparing Figures 25 and 18, the measured peak moisture content reached 14 percent moisture content with an air cavity and 24 percent moisture content with insulation in the cavity. Therefore, the presence of thermal insulation in the cavity increased the peak moisture content at the sugar pine by approximately 10 percent moisture content.

It was not possible to make a meaningful comparison for wall specimen 8 with cellulose insulation because the moisture content sensor at the inside wood surface malfunctioned during the experiment and gave unreasonably high values (i.e., considerably above fiber saturation). The presence of fire-retardant salts in the cellulose insulation caused the metered moisture content to read unreasonably high compared to the actual moisture content at the wood surface (Laurenzi 1994).

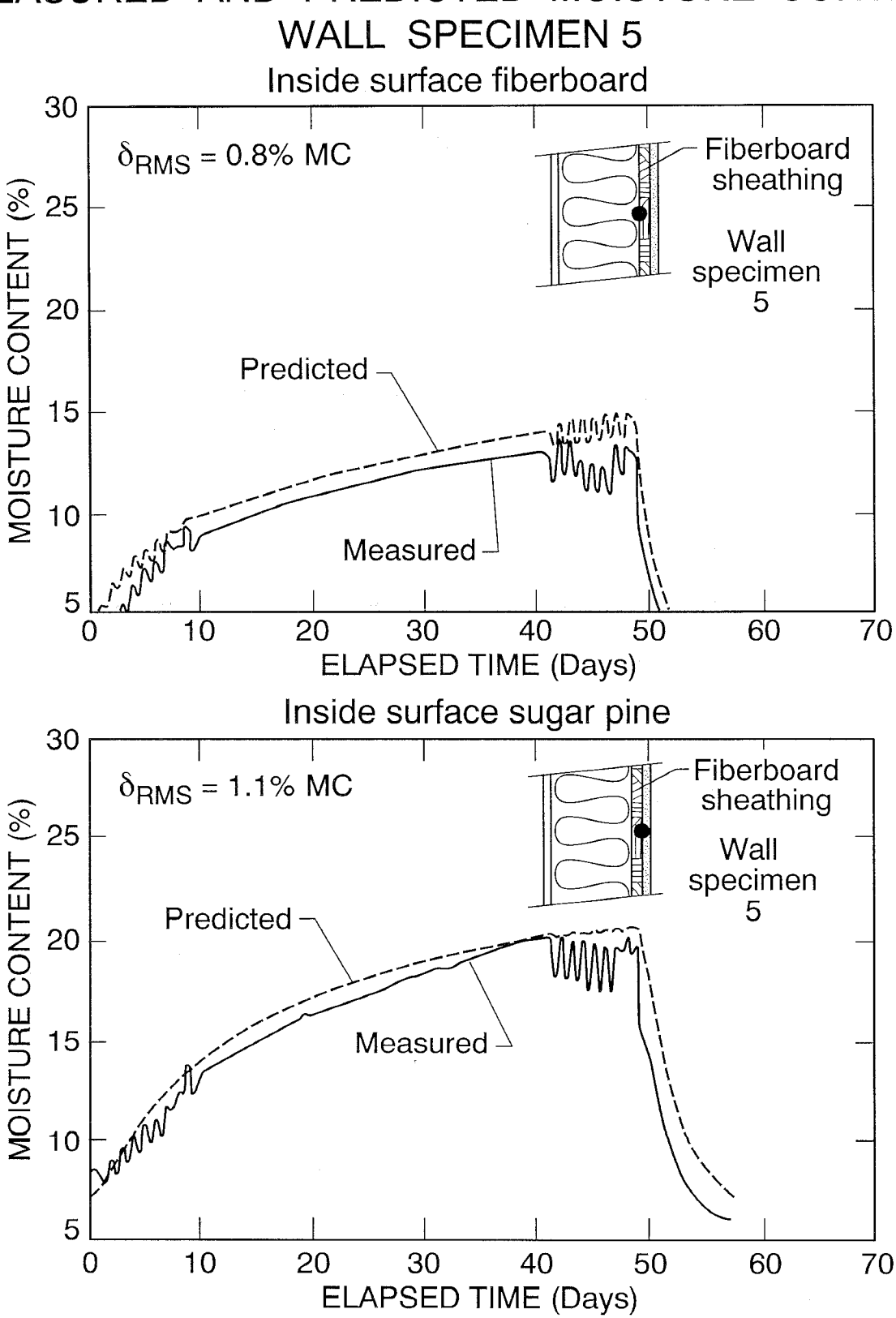
MEASURED AND PREDICTED MOISTURE CONTENT
WALL SPECIMEN 5
Inside surface fiberboard
δRMS = 0.8% MC
Fiberboard sheathing
Wall specimen 5
Predicted
Measured
MOISTURE CONTENT (%)
ELAPSED TIME (Days)
Inside surface sugar pine
δRMS = 1.1% MC
Fiberboard sheathing
Wall specimen 5
Predicted
Measured
MOISTURE CONTENT (%)
ELAPSED TIME (Days)

Figure 23

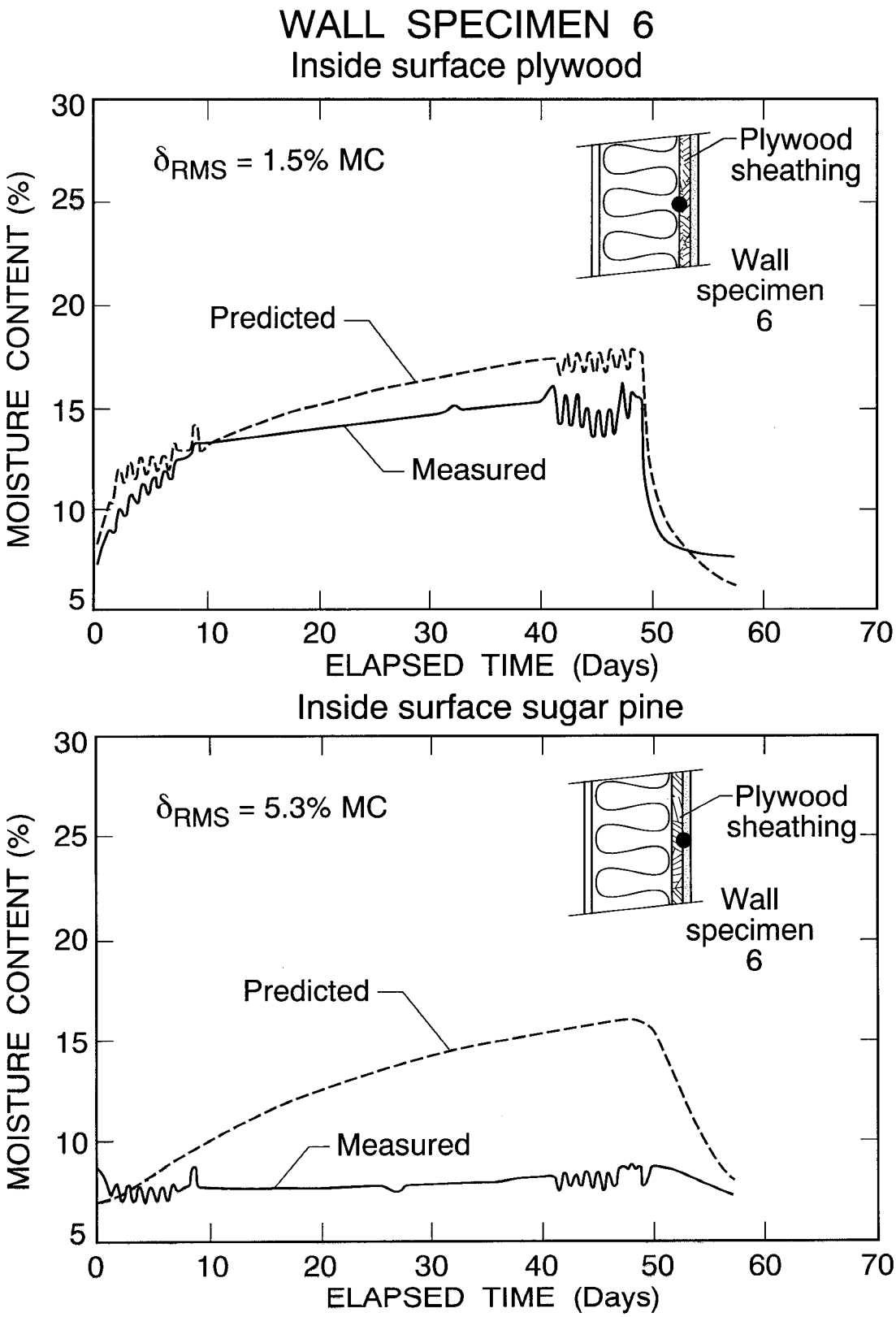
MEASURED AND PREDICTED MOISTURE CONTENT
WALL SPECIMEN 6
Inside surface plywood
$\delta_{RMS}$ = 1.5% MC
Plywood sheathing
Wall specimen 6
Predicted
Measured
MOISTURE CONTENT (%)
ELAPSED TIME (Days)
Inside surface sugar pine
$\delta_{RMS}$ = 5.3% MC
Plywood sheathing
Wall specimen 6
Predicted
Measured
MOISTURE CONTENT (%)
ELAPSED TIME (Days)

Figure 24

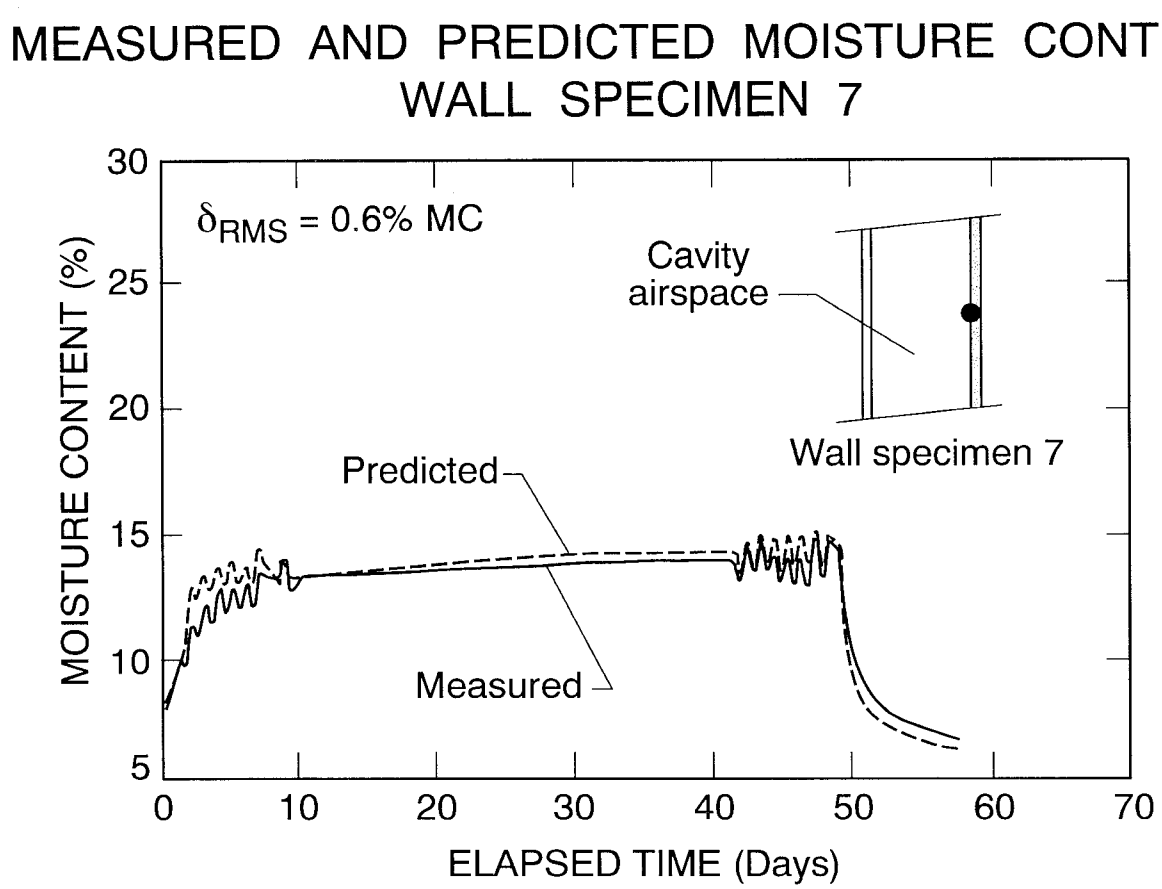
MEASURED AND PREDICTED MOISTURE CONTENT
WALL SPECIMEN 7
$\delta_{RMS}$ = 0.6% MC
Cavity airspace
Wall specimen 7
Predicted
Measured
MOISTURE CONTENT (%)
30
25
20
15
10
5
0
10
20
30
40
50
60
70
ELAPSED TIME (Days)

Figure 25

*Modeling Insulation as a Storage Layer*

For the comparisons of wall specimens 1 through 7, the cavity insulation was modeled as a nonstorage layer. In order to validate the capabilities of MOIST, a separate series of comparisons with the cavity insulation modeled as a storage layer were conducted. The agreement between measured and predicted results for these comparisons was comparable to the previous comparisons with the insulation modeled as a nonstorage layer. However, when the insulation was modeled as a storage layer, the authors encountered difficulty in achieving convergence of the MOIST predictions. It was necessary to specify a large number of finite-difference nodes (i.e., greater than 20) within the insulation layer in order to achieve convergence of the mathematical solution. Moreover, the MOIST predictions converged slowly to the exact solution as the number of nodes was increased. Consequently, this made it difficult to determine if a sufficient number of nodes were being used for convergence.

*Typical Wall Construction and Vapor Retarder Defects - Wall Specimens 9 to 12*

As mentioned above, wall specimens 9 through 12 were selected as representative of current building practice. The effect of a vapor retarder was investigated for these four walls. The walls were constructed of gypsum wallboard, glass-fiber insulation, foil-faced polyisocyanurate sheathing and vinyl siding. Wall specimens 9, 10, and 11 were constructed with a vapor retarder, whereas no vapor retarder was used on wall specimen 12. Wall specimens 10 and 11 were constructed purposely with a defect in the vapor retarder to simulate air leakage around an electric outlet. Moisture content sensors on a sugar pine substrate (Figure 8d), were placed at the center of each measurement section on the interior side of the polyisocyanurate sheathing.

The relative humidity at the interior surface of the polyisocyanurate sheathing was obtained by converting the measured output of the moisture content sensors using the sugar pine adsorption curves. The moisture content readings associated with wall specimen 11 were erroneous and are not presented. The resulting measured relative humidities for wall specimens 9, 10, and 12 are compared in Figure 26. Note that the surface relative humidity of wall specimen 12 (without vapor retarder) is saturated (100 percent) between the two sinusoidal conditions. On the other hand, the surface relative humidity for wall 9 (with a kraft-paper vapor retarder) rises to 92 percent during the same period. Use of the vapor retarder reduced the flow of water vapor into the wall resulting in a reduced water vapor pressure and relative humidity at the interior surface of the polyisocyanurate sheathing. It is interesting to note that the result for wall 10 (with a 11.5-mm hole in the vapor retarder) falls between the cases with and without a vapor retarder.

MOIST was used to predict the relative humidity at the interior surface of the polyisocyanurate sheathing of wall specimen 9 (with a kraft-paper vapor retarder). The predicted surface relative humidity (dashed line) is compared to the measured value (solid line) in Figure 27. There is generally good agreement between measured and predicted values, except during the diurnal sinewaves. During the sinusoidal conditions, the variation in amplitude of the MOIST predictions are considerably larger than those measured. This may be attributed to the time response of the moisture content sensors. A similar comparison is given in Figure 28 for wall

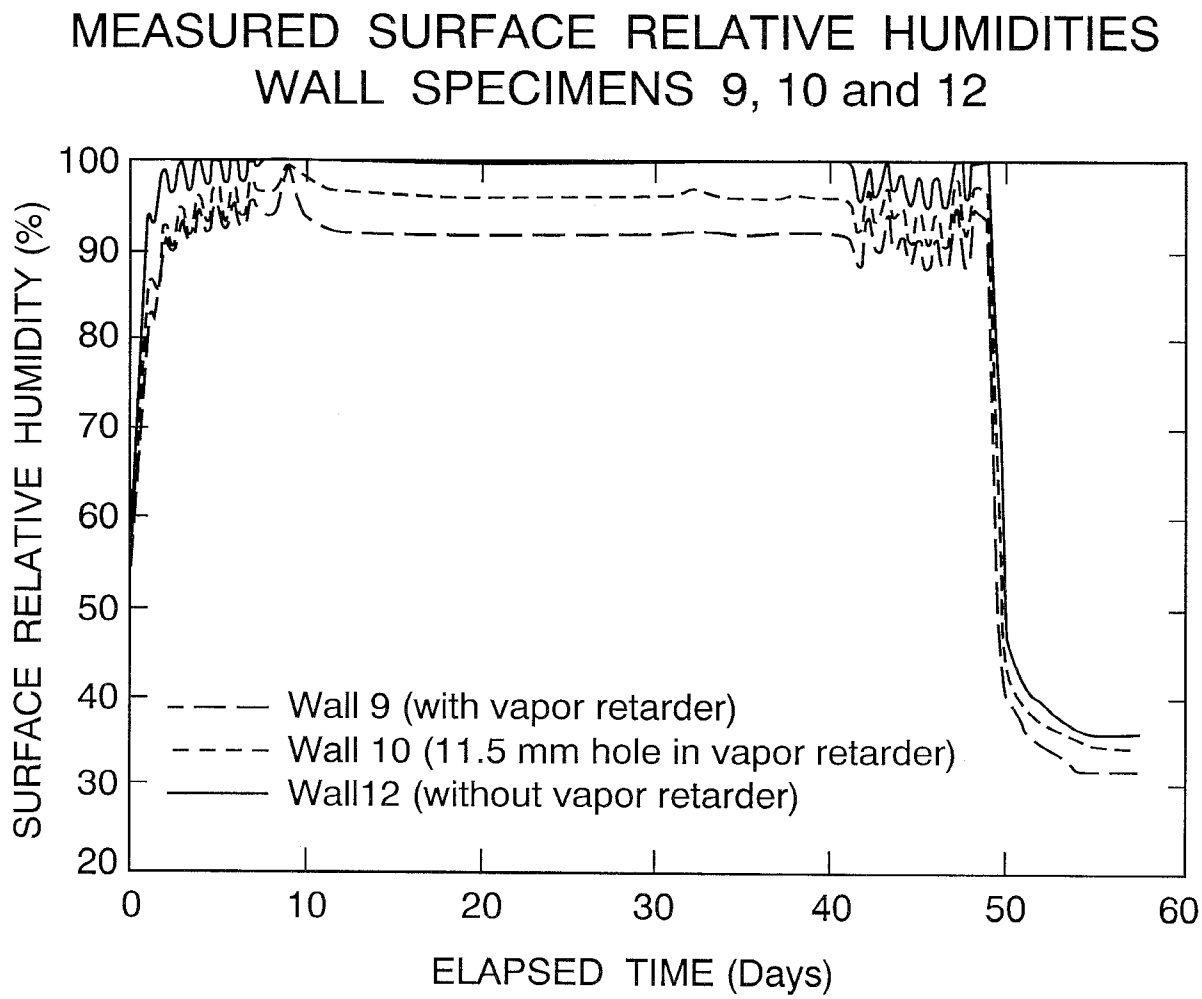
MEASURED SURFACE RELATIVE HUMIDITIES
WALL SPECIMENS 9, 10 and 12
SURFACE RELATIVE HUMIDITY (%)
100
90
80
70
60
50
40
30
20
0
10
20
30
40
50
60
ELAPSED TIME (Days)
Wall 9 (with vapor retarder)
Wall 10 (11.5 mm hole in vapor retarder)
Wall12 (without vapor retarder)

Figure 26

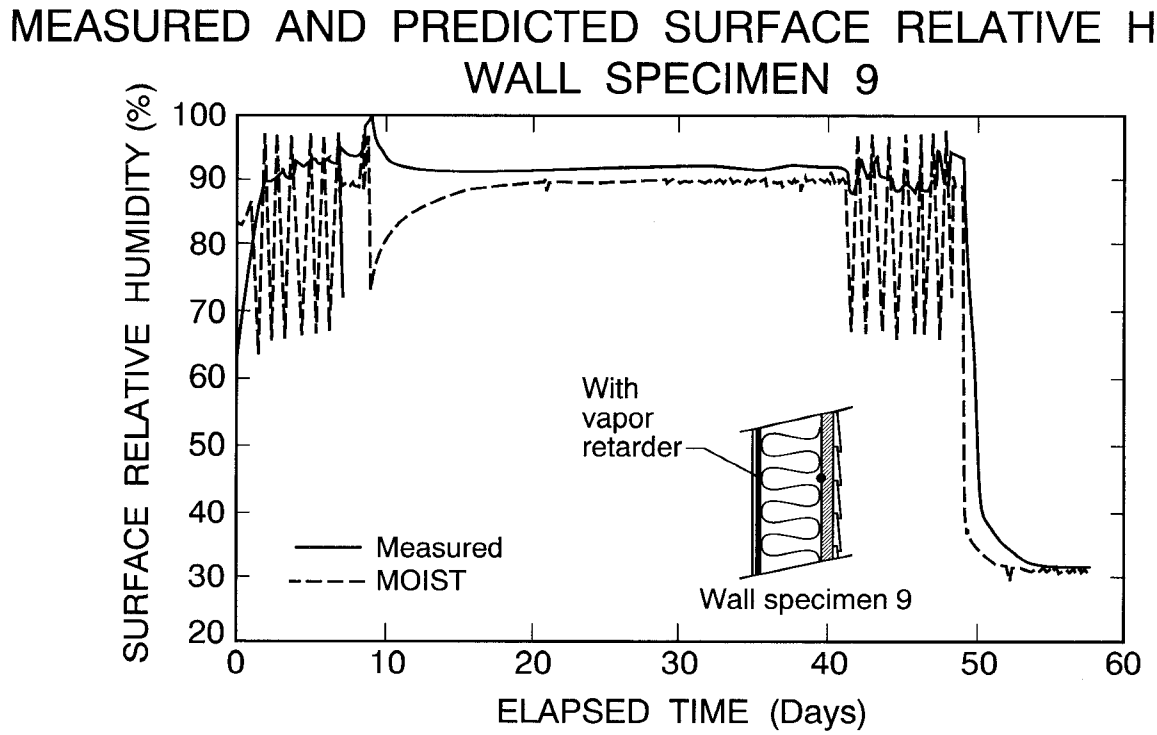


Figure 27

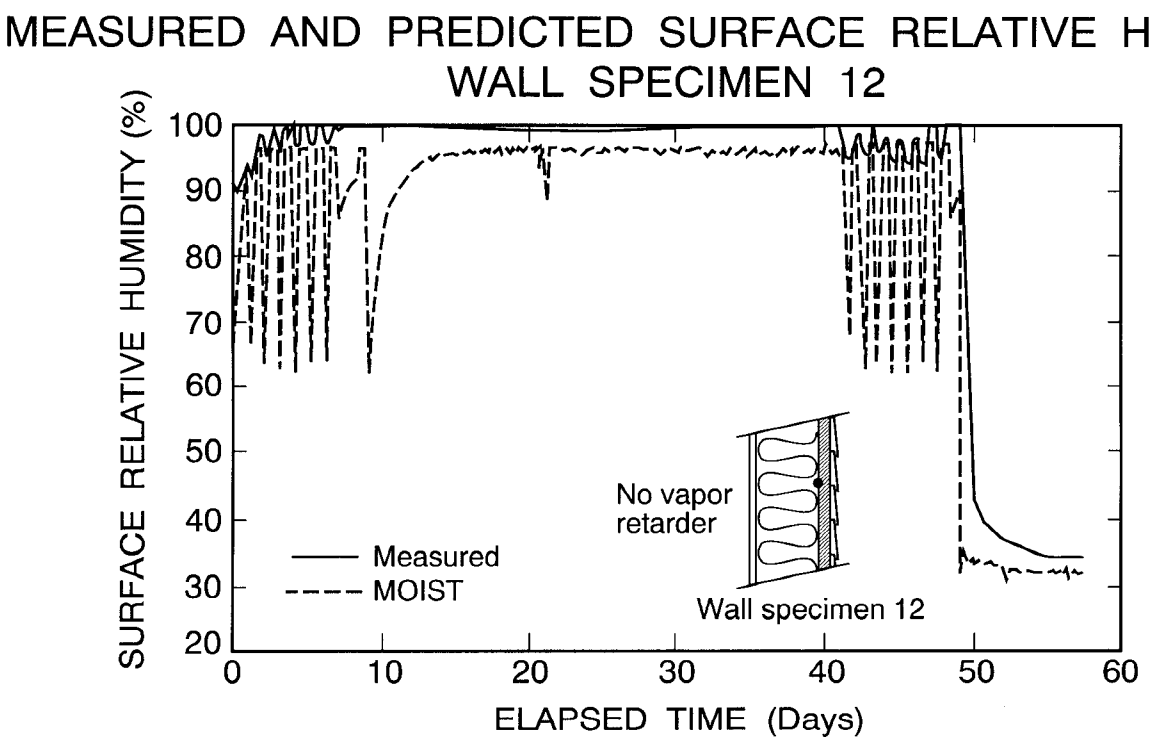


Figure 28

specimen 12 (without a vapor retarder). The agreement between measured and predicted values is again seen to be good. It was not possible to use MOIST to predict the response for wall specimens 10 and 11 because the penetrations in these walls caused significant departure from one-dimensional moisture transfer.

## Summary of Moisture Content Comparisons

The $\delta_{RMS}$ for wall specimens 1 through 7 is summarized in Table 10. Comparisons were not possible for wall specimen 8 due to the malfunctioning moisture content sensor. Wall specimens 9 through 12 did not include a hygroscopic sheathing or siding material and therefore moisture content comparisons were not made. With the exception of wall specimen 6, MOIST was able to predict the measured moisture contents with a maximum $\delta_{RMS}$ of 1.1 percent moisture content.

**Table 10**
**Summary of Root-Mean-Square Differences Between Measured and Predicted Moisture Contents**

| Wall Specimen | Wall Description (Parameter of Interest) | Root-Mean-Square Differences (%MC) |
|---|---|---|
| 1 | Base case | 1.1 |
| 2 | Vapor retarder of kraft paper and asphalt mastic | 0.9 |
| 3 | Interior latex paint and exterior oil-base paint | 0.5 |
| 4 | Interior and exterior latex paint | 1.1 |
| 5 | Fiberboard sheathing<br>• Inside sheathing surface<br>• Inside wood surface | <br>0.8<br>1.1 |
| 6 | Plywood sheathing<br>• Inside sheathing surface<br>• Inside wood surface | <br>1.5<br>5.3 |
| 7 | Cavity airspace | 0.6 |

## Heat Flux Comparisons

The heat flux measured by the heat flux transducers at the inside surface of the twelve wall specimens was compared to corresponding values predicted by MOIST. For the computer predictions, the glass-fiber insulation was again modeled as a nonstorage layer (i.e., the storage of heat and moisture was neglected). The measured and predicted heat flux for wall specimen 1

were compared for the entire test period as shown in Figure 29. At time zero, the air temperature at the exterior surface was decreased suddenly (fig. 5) causing, in this case, a positive heat flux at the interior surface (i.e., a heat loss). The large fluctuations in heat flux during days 1 to 7 and 41 to 48 were caused by the diurnal sinewaves of the exterior air temperature. After 48 days, the exterior air temperature was suddenly increased to 32 °C causing the heat flux to change abruptly to a negative value (i.e., a heat gain). As observed in Figure 29, the heat flux predicted by MOIST tracks the measured heat flux. However, the long-time scale and the close proximity of the two curves make it difficult to ascertain the level of agreement. In-depth comparisons are examined below to assess the accuracy of MOIST heat flux predictions.

For a one-week steady-state period proceeding the second series of sinewaves, the measured and predicted heat fluxes for the 12 wall specimens were averaged and compared. The results are given in Figure 30 as a series of bar graphs. The first bar gives the measurement by the heat flux transducer; the second, the prediction by MOIST. The agreement was within $\pm 10$ percent. The differences between measured and predicted values are summarized in Table 11.

**Table 11**
**Comparison of Steady Heat Fluxes ($W/m^2$)**

| Wall Specimen | Measured ($W/m^2$) | MOIST ($W/m^2$) | Difference (%) |
|---|---|---|---|
| 1 | 6.24 | 5.93 | −5.0 |
| 2 | 5.76 | 6.05 | 5.0 |
| 3 | 5.30 | 5.84 | 10.2 |
| 4 | 6.71 | 7.09 | 5.6 |
| 5 | 5.19 | 5.40 | 4.0 |
| 6 | 6.04 | 6.33 | 4.6 |
| 7 | 21.5 | 20.02 | −6.9 |
| 8 | 6.04 | 5.46 | −9.6 |
| 9 | 5.32 | 5.11 | −3.9 |
| 10 | 4.34 | 4.70 | 8.3 |
| 11 | 4.81 | 4.79 | −0.4 |
| 12 | 4.65 | 5.08 | 9.2 |

# MEASURED AND PREDICTED HEAT FLUX WALL SPECIMEN 1

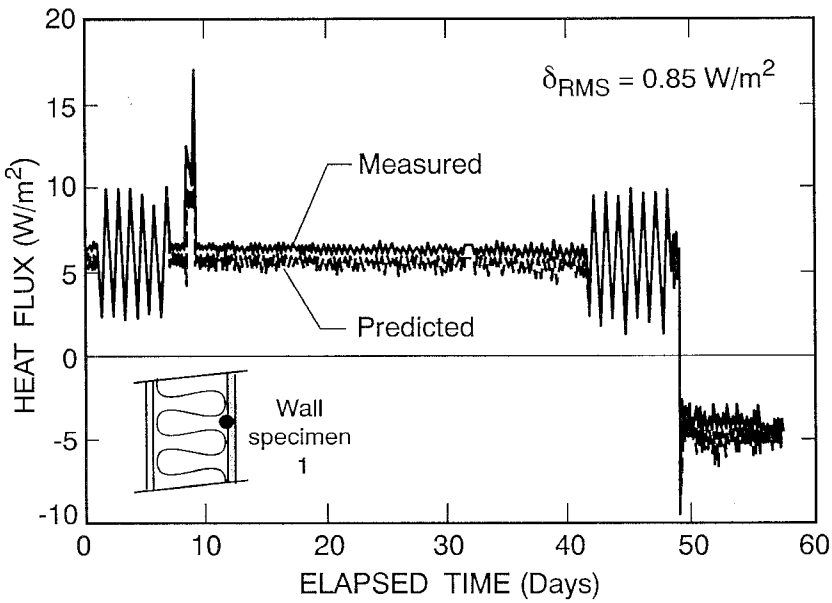


Figure 29

# COMPARISON BETWEEN MEASURED AND PREDICTED STEADY-STATE HEAT FLUXES

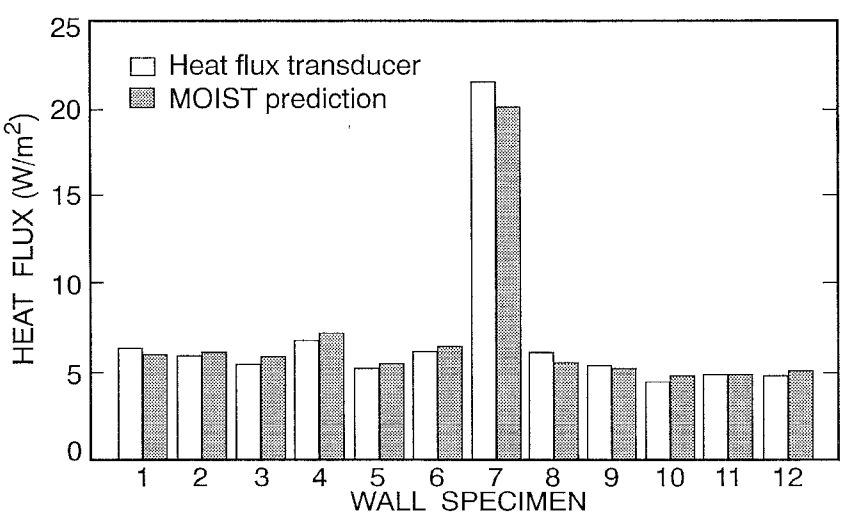


Figure 30

For the second series of diurnal sinewaves, a comparison of the measured and predicted time-dependent heat fluxes for wall specimens 1 through 12 is given in Figure 31. The $\delta_{RMS}$ given in each of the plots is summarized in Table 12. The above comparisons show very good agreement between measured and predicted time-dependent heat fluxes. The $\delta_{RMS}$ is expressed in absolute units of $W/m^2$. If we divide the $\delta_{RMS}$ by the mean heat flux, then the $\delta_{RMS}$ may be expressed as a percentage which ranges from 4 to 15 percent.

**Table 12**
**Summary of Root-Mean-Square Differences Between Measured and Predicted Heat Fluxes**

| Wall Specimen | Root-Mean-Square Differences ($W/m^2$) |
|---|---|
| 1 | 0.68 |
| 2 | 0.78 |
| 3 | 0.72 |
| 4 | 0.65 |
| 5 | 0.69 |
| 6 | 0.77 |
| 7 | 1.44 |
| 8 | 0.88 |
| 9 | 0.19 |
| 10 | 0.56 |
| 11 | 0.22 |
| 12 | 0.56 |

# MEASURED AND PREDICTED HEAT FLUXES

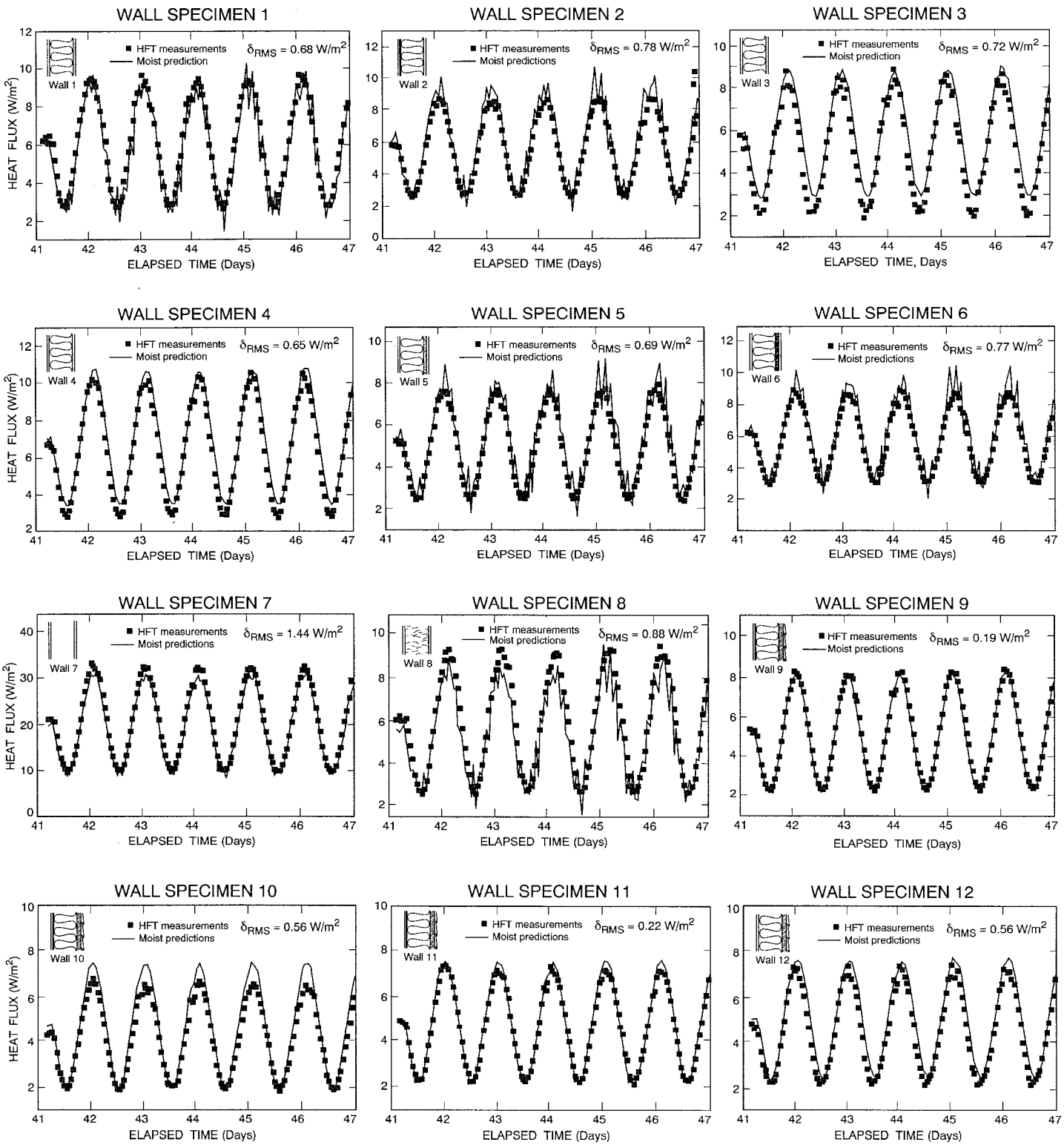


Figure 31

# COMPARISONS OF MOIST AND TARP

In order to provide another independent verification of the accuracy of the heat transfer algorithms of MOIST, simulations of MOIST and the Thermal Analysis Research Program, TARP (Walton 1983), were compared. TARP is a computer program developed at NIST to compute space heating and cooling loads for buildings. The program can compute sensible heat transfer at interior surfaces of buildings, but does not account for either moisture transfer or the latent heat effect due to adsorbed and desorbed moisture. Therefore, in order to make the comparisons meaningful, a vapor impermeable paint layer was included in the MOIST geometry. For boundary conditions, a constant interior air temperature of 21.15 °C and the exterior air temperature from the calibrated hot box experiment were input for both programs. The interior heat flux predicted by MOIST and TARP for the first seven days of the experiment are compared in Figure 32 for wall specimen 1. The good agreement between MOIST and TARP provides another independent verification of the heat transfer algorithms of MOIST.

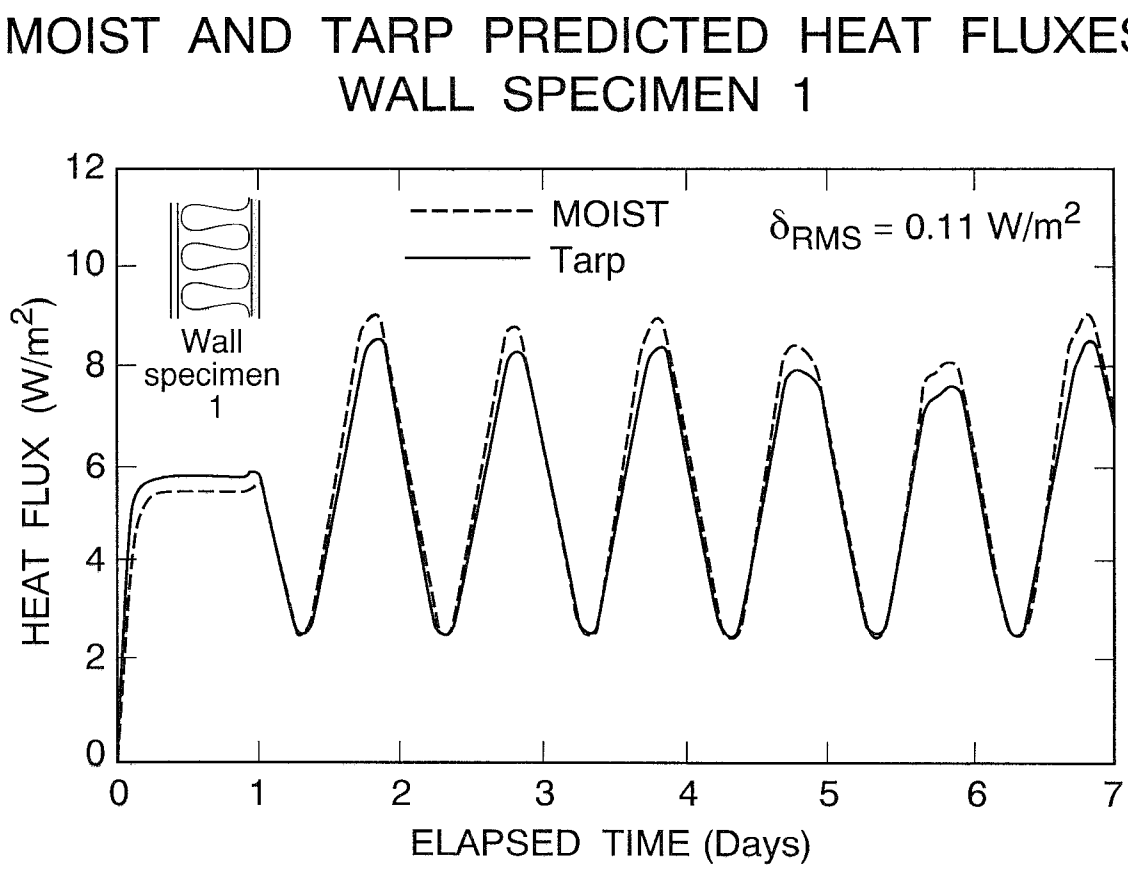
MOIST AND TARP PREDICTED HEAT FLUXES
WALL SPECIMEN 1
MOIST
Tarp
$\delta_{RMS}$ = 0.11 W/m$^2$
Wall specimen 1
HEAT FLUX (W/m$^2$)
ELAPSED TIME (Days)
0
2
4
6
8
10
12
0
1
2
3
4
5
6
7

Figure 32

# COMPARISON OF STEADY-STATE HEAT FLUX MEASUREMENTS TO ASHRAE PREDICTIONS

Additional comparisons were performed to determine the effectiveness of simple hand calculations for predicting the steady-state heat flux through the wall specimens. In this case, the measured steady-state heat flux was compared to values calculated using procedures outlined in the ASHRAE Handbook of Fundamentals (ASHRAE 1993). Following the ASHRAE procedure, the overall thermal resistance for each wall specimen was calculated by summing the thermal resistance of each individual layer of construction and the thermal resistance due to the inside and outside air film coefficients or:

$$R_T = \frac{1}{h_i} + \sum_{j=1}^{J} R_j + \frac{1}{h_o} . \tag{7}$$

Here, J was equal to 3 or 4 depending on the number of material layers used in the construction of the wall specimen. The thermal resistance of each layer was determined by:

$$R_j = \frac{L_j}{\lambda_j} . \tag{8}$$

By modifying the combined (free and forced) convection equation for a 0.5 $m^2$ plate (Duffie and Beckman 1991) to include the effects of natural convection, forced convection, and radiation, the following equation was developed for the inside and outside air film coefficients:

$$h_{i,o} = a\,|\Delta T_{air}|^{\frac{1}{3}} + b v_{air} + 4\epsilon\sigma T_m^{\,3} . \tag{9}$$

In our experimental set-up, the surface temperatures were not measured in every case. Consequently, $\Delta T_{air}$ and $T_m$ were not known and had to be calculated. The thermal transmittance and heat flux through each wall specimen were computed from the following equations:

$$U = \frac{1}{R_T} , \tag{10}$$

$$q = U(T_i - T_o) . \tag{11}$$

To determine q, eqs (7-11) were prepared and solved simultaneously for each wall specimen. The input data for the inside and outside air temperatures and velocities were obtained from the calibrated hot box experiment for days 10 through 14. For most of the wall materials, the thicknesses and thermal conductivities were obtained from the results of the guarded hot plate tests (Table 8). The values of thermal conductivity for the glass-fiber thermal insulation were taken from Table 9 and accounted for the in situ density as installed in the wall specimen. For the vinyl-lapped siding and the cavity airspace (wall specimen 7), thermal resistance values of 0.13 and 0.17 $m^2 \cdot K/W$, respectively, were obtained (ASHRAE 1993). The input data, computed thermal resistance, transmittance, and heat flux for each wall specimen are summarized in Table 13.

As anticipated, the most pronounced result of the analysis was the effect of installing thermal insulation within the cavity airspace. The thermal resistance of wall specimen 7 (cavity airspace) was approximately three times less than similar constructions with insulation. Consequently, the heat flux through this specimen was about three times greater than the other wall specimens. The specimen heat flux was also decreased by the addition of a layer of sheathing. Using wall specimen 1 as the basis, the addition of plywood was found to increase the overall thermal resistance by 7 percent; fiberboard, by 10 percent; and, polyisocyanurate foam, by 25 percent. Note that the variations in heat flux for specimens with glass-fiber thermal insulation were caused by the local density variations of the glass-fiber insulation.

The measured thermal resistance for each wall specimen was computed for days 10 through 14 (120 hours) of the winter test condition, the same interval used for the ASHRAE calculations. For this interval, the measured thermal resistance of each wall specimen was determined by dividing the summation of the (air) temperature difference across the wall specimen by the summation of the heat flux from the heat flux transducer, or:

$$R_{HFT} = \frac{\sum_{t=1}^{120} \Delta T_t}{\sum_{t=1}^{120} q_t} . \qquad (12)$$

The differences between the measured and predicted values are summarized in Table 14 and plotted in Figure 33. In general, the differences ranged from −13 to +5 percent.

**Table 13**
**Steady-State Thermal Transmission Properties and Predicted Heat Fluxes**

| Wall | Experimental Inside Air Temperature (°C) | Calculated Inside Film Coefficient ($W/m^2K$) | Thermal Resistance Layer 1 ($m^2 \cdot K/W$) | Thermal Resistance Layer 2 ($m^2 \cdot K/W$) | Thermal Resistance Layer 3 ($m^2 \cdot K/W$) | Thermal Resistance Layer 4 ($m^2 \cdot K/W$) | Calculated Outside Film Coefficient ($W/m^2 \cdot K$) | Experimental Outside Air Temperature (°C) | Thermal Resistance ($m^2 \cdot K/W$) | Thermal Transmittance ($W/m^2 \cdot K$) | Heat Flux ($W/m^2$) |
|---|---|---|---|---|---|---|---|---|---|---|---|
| 1 | 21.2 | 6.5 | 0.08 | 1.83 | 0.21 | - | 8.2 | 7.3 | 2.40 | 0.417 | 5.77 |
| 2 | 21.2 | 6.5 | 0.08 | 1.84 | 0.21 | - | 8.2 | 7.1 | 2.41 | 0.416 | 5.87 |
| 3 | 21.1 | 6.5 | 0.08 | 1.91 | 0.21 | - | 8.2 | 7.0 | 2.48 | 0.403 | 5.68 |
| 4 | 21.1 | 6.6 | 0.08 | 1.50 | 0.21 | - | 8.2 | 6.8 | 2.07 | 0.483 | 6.91 |
| 5 | 21.2 | 6.4 | 0.08 | 1.81 | 0.25 | 0.21 | 8.7 | 7.3 | 2.62 | 0.382 | 5.31 |
| 6 | 21.2 | 6.5 | 0.08 | 1.53 | 0.17 | 0.21 | 8.8 | 7.1 | 2.26 | 0.442 | 6.22 |
| 7 | 21.1 | 7.2 | 0.08 | 0.17 | 0.21 | - | 8.9 | 7.0 | 0.72 | 1.396 | 19.66 |
| 8 | 21.2 | 6.4 | 0.08 | 2.12 | 0.21 | - | 8.1 | 6.7 | 2.69 | 0.371 | 5.38 |
| 9 | 21.3 | 6.4 | 0.08 | 1.74 | 0.61 | 0.13 | 8.4 | 7.2 | 2.83 | 0.353 | 4.96 |
| 10 | 21.3 | 6.4 | 0.08 | 1.93 | 0.61 | 0.13 | 8.4 | 7.0 | 3.02 | 0.331 | 4.71 |
| 11 | 21.3 | 6.4 | 0.08 | 1.95 | 0.61 | 0.13 | 8.4 | 6.9 | 3.04 | 0.329 | 4.74 |
| 12 | 21.3 | 6.4 | 0.08 | 1.86 | 0.61 | 0.13 | 8.4 | 6.7 | 2.95 | 0.339 | 4.95 |

| Table 14<br>R-Value Comparison for Days 10 through 14 | | | | |
|---|---|---|---|---|
| **Wall Specimen** | **ASHRAE ($m^2 \cdot K/W$)** | **Measured ($m^2 \cdot K/W$)** | **Difference ($m^2 \cdot K/W$)** | **Difference (%)** |
| 1 | 2.40 | 2.17 | -0.23 | -9.6 |
| 2 | 2.41 | 2.37 | -0.04 | -1.5 |
| 3 | 2.48 | 2.58 | 0.10 | 4.2 |
| 4 | 2.07 | 2.07 | 0.00 | 0.0 |
| 5 | 2.62 | 2.58 | -0.04 | -1.6 |
| 6 | 2.26 | 2.23 | -0.03 | -1.5 |
| 7 | 0.72 | 0.63 | -0.09 | -12.6 |
| 8 | 2.69 | 2.40 | -0.29 | -10.7 |
| 9 | 2.83 | 2.62 | -0.21 | -7.6 |
| 10 | 3.02 | 3.17 | 0.15 | 5.1 |
| 11 | 3.04 | 2.92 | -0.12 | -4.1 |
| 12 | 2.95 | 3.04 | 0.09 | 2.9 |

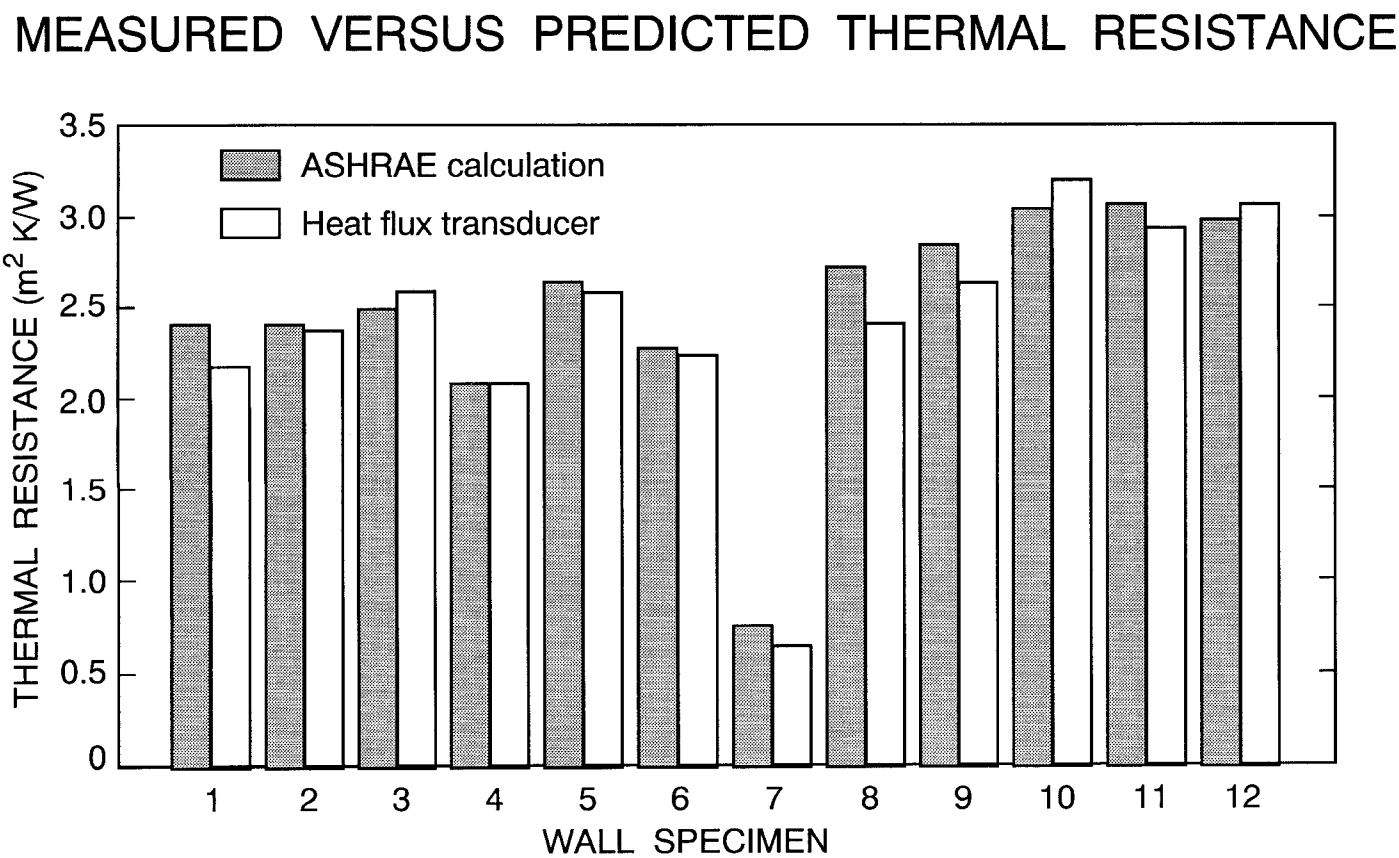
MEASURED VERSUS PREDICTED THERMAL RESISTANCE
ASHRAE calculation
Heat flux transducer
THERMAL RESISTANCE (m2 K/W)
3.5
3.0
2.5
2.0
1.5
1.0
0.5
0
1
2
3
4
5
6
7
8
9
10
11
12
WALL SPECIMEN

Figure 33

# EFFECT OF MOISTURE ON HEAT TRANSFER

The effect of moisture on heat transfer was investigated by comparing the measured heat fluxes from the first and second series of diurnal sinewaves. These sinewaves were separated by a 34-day steady-state winter condition in which moisture accumulated in the hygroscopic sheathing and siding materials. Thus, the wall specimens were comparatively "dry" during the first series of diurnal sinewaves because insufficient time had elapsed for moisture to accumulate. However, by the second series, a considerable amount of moisture had accumulated in the sheathing and siding. To accentuate the potential effect, two wall specimens without a vapor retarder were selected for the comparison, wall specimen 1 (glass-fiber cavity insulation) and wall specimen 8 (cellulose cavity insulation).

The exterior air temperatures for the first and second series of diurnal sinewaves are compared for 4 days in Figure 34. The two waveforms are nearly the same, varying from 1.1 to 15.6 °C. During both periods, the interior air temperature was maintained at 21.2 $\pm$ 0.1 °C. The corresponding diurnal heat fluxes for wall specimens 1 and 8 are shown in Figure 35. The waveforms are nearly the same, indicating that for these temperatures (note that there was no reversal in heat flux) moisture accumulation had little or no effect on the heat transfer. Although considerable moisture had accumulated in the sugar pine of the wall specimens (fig. 19), the level was below the fiber saturation point. Therefore, no liquid water was in the pore space of the materials. The authors recognize that under other temperature conditions when liquid water is present in construction, latent heat can have a large effect on heat transfer (Hedlin 1988).

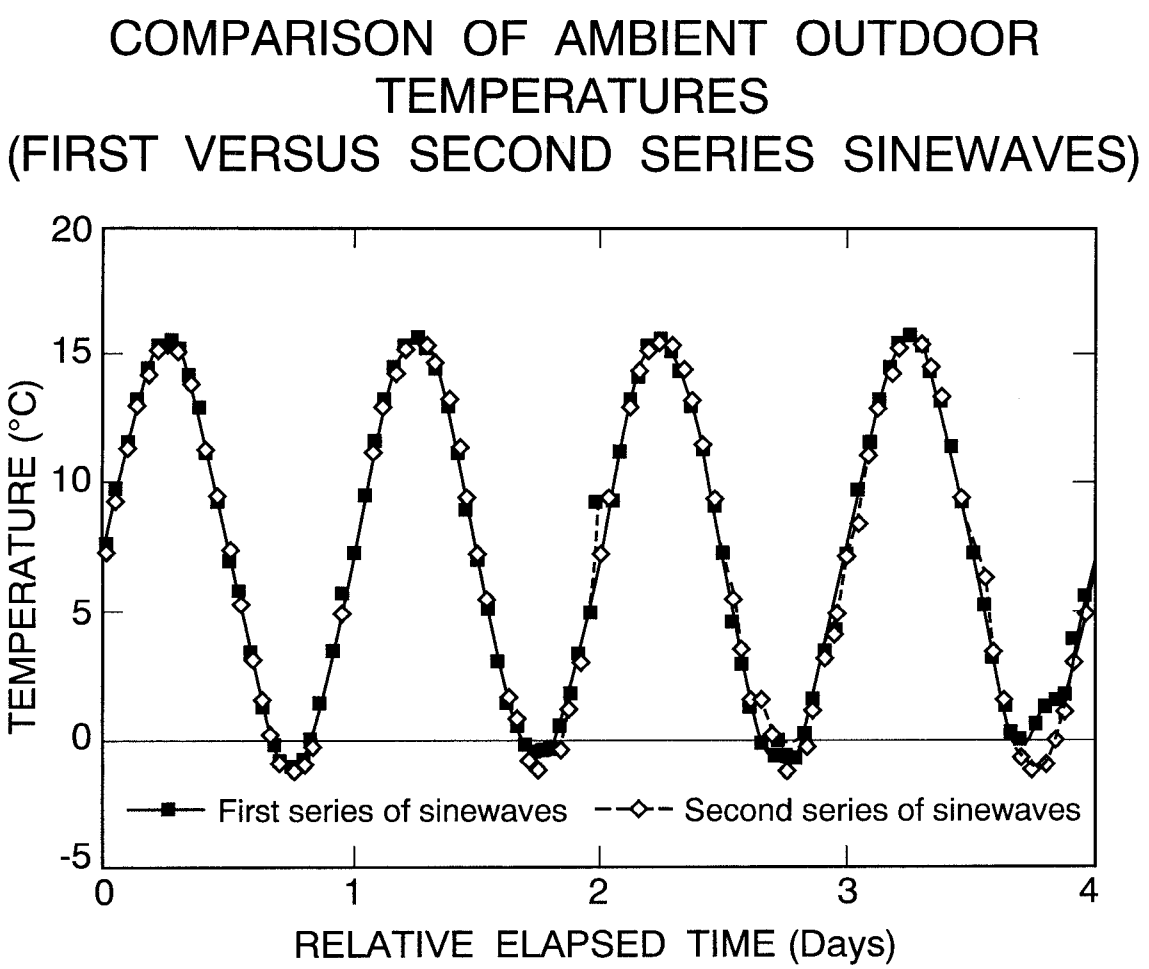
COMPARISON OF AMBIENT OUTDOOR TEMPERATURES
(FIRST VERSUS SECOND SERIES SINEWAVES)
20
15
10
5
0
-5
TEMPERATURE (°C)
First series of sinewaves
Second series of sinewaves
0
1
2
3
4
RELATIVE ELAPSED TIME (Days)

Figure 34

# COMPARISON OF HEAT FLUXES (FIRST VERSUS SECOND SERIES SINEWAVES)

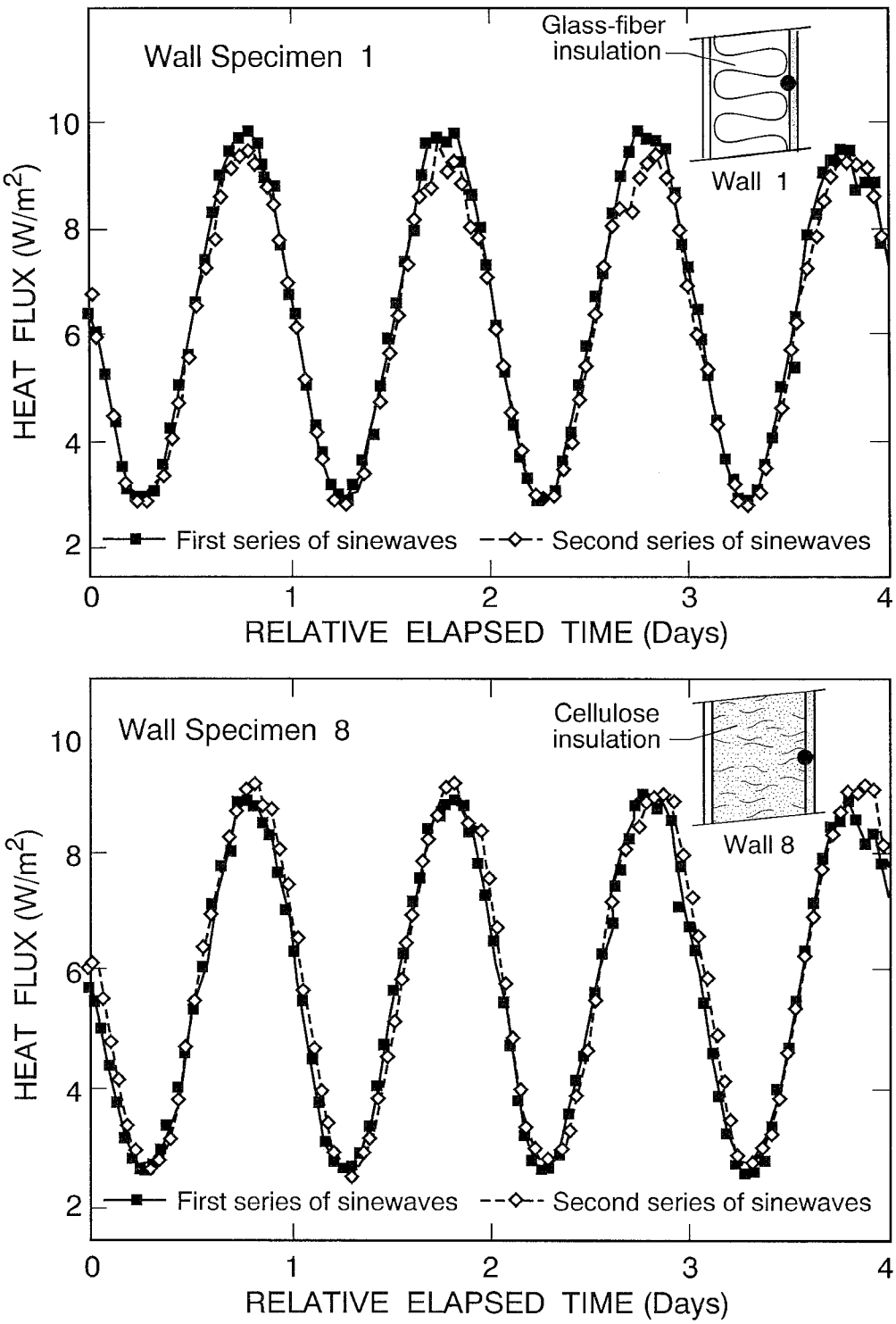


Figure 35

# SUMMARY AND CONCLUSIONS

A comprehensive laboratory study was conducted to verify the accuracy of MOIST, a personal computer program that predicts the transient one-dimensional heat and moisture transfer in building envelopes. The rate of heat transfer and moisture content of twelve wall specimens, typical of residential wood-frame construction, were measured and subsequently compared to simulations by MOIST. In addition, the steady-state heat fluxes of each wall specimen were compared to values calculated using procedures outlined in the ASHRAE Handbook of Fundamentals.

The twelve wall specimens were assembled collectively in the NIST calibrated hot box and exposed to both steady-state and transient temperature conditions over a continuous period of 104 days. Eight of the wall specimens were designed to examine the relative effects of different constructions on the accumulation of moisture in the wall specimen. The other four specimens investigated the effectiveness of vapor retarders in controlling the movement of moisture. The interior ambient air was maintained at fixed levels of temperature and relative humidity during the experiment. The exterior ambient air was varied to promote moisture accumulation in the specimens during transient and steady winter conditions and drying during the steady summer condition.

Each wall specimen was constructed with an isolated circular meter section in order to promote one-dimensional moisture transfer through the specimen. The rate of heat transfer through each specimen was measured using a single heat flux transducer located at the interior surface of the wall specimen. The moisture content of selected building materials within the specimen was determined using electrical-resistance moisture content sensors. An extensive calibration was conducted to provide an individual calibration for each heat flux transducer and moisture content sensor. Results of the moisture content sensor calibration showed significant sensor-to-sensor variability indicating serious errors would have occurred if only a single sensor calibration had been used.

MOIST simulations were conducted using the same boundary conditions as those imposed on the wall specimens during the calibrated hot box experiment. In addition, to minimize the uncertainties associated with material variability, the material properties - sorption isotherm, permeability, and thermal conductivity - were measured for each of the materials used in the wall specimens. Comparisons were conducted for eight wall specimens instrumented with moisture content sensors in their exterior hygroscopic materials. In general, the agreement between predicted and measured moisture content was good. For six of these walls, the root-mean-square differences were less than 1.1 percent moisture content. The largest difference was 5.3 percent moisture content for a wall specimen with plywood sheathing. A comparison with a wall specimen that contained cellulose loose-fill insulation was not possible because the sensor failed.

The other four walls were constructed with a sheathing layer of foil-faced polyisocyanurate foam. Here, moisture content sensors on a sugar pine substrate were applied and used to determine the relative humidity at the interior surface of the sheathing. The measured relative humidities were in close agreement with those predicted by MOIST. For the interior and exterior ambient conditions used in the experiment, the inclusion of a vapor retarder did not significantly reduce the relative humidity at the interior surface of the sheathing. If climatic conditions had existed in which the interior surface of the sheathing was below the dew point of interior air, then the presence of a vapor retarder would have had a larger effect on the moisture content of the building materials.

In general, the values of heat flux predicted by the MOIST simulations were in good agreement with the measured values. For the twelve wall specimens, the predictions of steady-state heat flux were within 10 percent of the measured values. During the transient portion of the experiment, the root-mean-square differences between the predicted and measured values for the 12 specimens ranged from 4 to 15 percent. The predicted values of heat flux from the MOIST simulations were also in good agreement with the predictions of the Thermal Analysis Research Program, a computer program for building and cooling load simulations. The measured steady-state heat flux of the twelve wall specimens ranged from $-13$ to $+5$ percent of the values predicted using the procedures outlined in the ASHRAE Handbook of Fundamentals. For these particular experiments, moisture was found to have an insignificant effect on heat transfer.

# ACKNOWLEDGMENTS

We appreciate discussions with the following reviewers: Dale Bentz, Dr. Walter Rossiter at NIST and Dr. William C. Thomas at the Virginia Polytechnic Institute and State University. Their comments greatly improved the report. We also acknowledge the following persons and contributions. The wall specimens were constructed under the supervision of Donn Ebberts with assistance from John Judge. Programming for data acquisition was provided by Kevin Simmons. Daily monitoring of the calibrated hot box during testing was provided by Kenneth Kramp and Daniel Shapiro. The moisture content sensors were calibrated by Kenneth Kramp and Holly Chandler. We also thank Kimberly Whitter for preparing this manuscript for publication.

# REFERENCES


Achenbach, P.R., "Design of a Calibrated Hot Box for Measuring the Heat, Air and Moisture of Composite Building Walls," ASHRAE Special Publication 28. 1979 December. pp. 308-319.

Annual Book of ASTM Standards, Thermal Insulation; Environmental Acoustics; Vol. 04.06. Philadelphia: ASTM, 1994.

ASHRAE Handbook of Fundamentals. Atlanta: American Society of Heating, Refrigerating and Air-Conditioning Engineers, Inc, 1993.

Bales, E. and Rose, W.B., Eds., Bugs, Mold & Rot, Workshop Proceedings, May 1991.

Boulant, J., Langlais, C. and Klarsfeld, S., "Correlation Between the Structural Parameters and the Thermal Resistance of Fibrous Insulants at High Temperatures," Seventeenth International Thermal Conductivity Conference. 1983. pp. 381-392.

Burch, D.M. and Thomas, W.C., "An Analysis of Moisture Accumulation in a Wood Frame Wall Subjected to Winter Climate," NISTIR 4674, National Institute of Standards and Technology. 1991 October.

Burch, D.M. and Thomas, W.C., "MOIST– A PC Program for Predicting Heat and Moisture Transfer in Building Envelopes," NIST Special Publication 853, National Institute of Standards and Technology. 1993.

Burch, D.M., Thomas, W.C. and Fanney, A.H., "Water Vapor Permeability Measurements of Common Building Materials," ASHRAE Transactions. 1992. Vol. 98, Pt.2.

Crow, L.W., "Development of Hourly Data for Weather Year for Energy Calculations (WYEC)," ASHRAE Journal. 1981 October. Vol. 23, No. 10, pp. 37-41.

Duff, J.E., "Moisture Distribution In Wood-Frame Walls in Winter," Forest Products Journal. 1968 January. Vol. 18, No. 1.

Duffie, J.A. and Beckman, W.A., Solar Engineering of Thermal Processes. John Wiley & Sons, Inc., 1991. p174.

Greenspan, L., "Humidity Fixed Points of Binary Saturated Aqueous Solutions," Journal of Research, National Bureau of Standards. 1977. Vol. 81A, pp.89-96.

Laurenzi, P., Personal Communication, Delmhorst Instrumentation Company, September 1994.

Hasegawa, S., Little, J.W., "The NBS Two-Pressure Humidity Generator, Mark 2," Journal of Research of the National Bureau of Standards - A. Physics and Chemistry. 1976 January-February. Vol. 81A, No. 1.

Hedlin, C.P., "Heat Flow Through a Roof Having Moisture Contents Between 0 and 1% by Volume in Summer," ASHRAE Transactions Part 2, pp. 1579-1599.

Hittle, D.C., "BLAST, The Building Loads Analysis and System Thermodynamics Program," CERL-TR-E-119, U.S. Army Construction Engineering Research Laboratory, 1977.

Kreith, F., Principles of Heat Transfer, International Textbook Company, 1968, pp. 550-556.

Rennex, B.G., "Error Analysis for the National Bureau of Standards 1016 mm Guarded Hot Plate," Journal of Thermal Insulation. 1983 July. Vol. 7, pp. 18-51.

Richards, R.F., Burch, D.M. and Thomas, W.C., "Water Vapor Sorption Measurements of Common Building Materials," ASHRAE Transactions. 1992. Vol. 98, Pt. 2.

Semerjian, H.G., "Report of Calibration, Thermocouple Type−T," NIST Test No. 311-4-91. 1991.

Threlkeld, J.L., Thermal Environmental Engineering. Prentice-Hall, Inc., 1970. pp. 196-198.

Walton, G.N., "Thermal Analysis Research Program - Reference Manual," NBSIR 83-2655, National Bureau of Standards. 1983.

Watmuff, J.H., Charters, W.W.S. and Proctor, D., "Solar and Wind Induced External Coefficients for Solar Collectors," COMPLES. 1977. No. 2, 56.

Zarr, R.R., Burch, D.M., Faison, T.K., Arnold, C.E. and O'Connell, M.E., "Calibration of the NBS Calibrated Hot Box," ASTM Journal of Testing and Evaluation. 1987 May. Vol. 15, No. 3, pp. 167-177.

# APPENDIX A

## BUILDING MATERIALS

1) *Cellulose*—loose-fill insulation comprised mostly of macerated paper, chemically treated with fire retardants. The cellulose was hand installed in the wall cavity at a nominal density of 56 kg/m$^3$ (3.5 lb/ft$^3$).

2) *Fiberboard, intermediate grade*—12.7 mm ($^1/_2$ in.) rigid board comprised of small lignin and cellulosic fibers (usually wood or cane) interfelted for intermediate type exterior sheathing (see ASTM Specification C 208). This particular product contained an added binder, probably asphalt.

3) *Glass-fiber insulation*—fibrous-glass batt cavity insulation with phenolic binder. Two types were acquired. The first type was manufactured without a vapor retarder (i.e., no backing) and the second type was manufactured with a vapor retarder of kraft paper with asphalt mastic.

4) *Gypsum wallboard*—12.7 mm ($^1/_2$ in.) interior sheathing of essentially gypsum core with paper bonded to the core (see ASTM Specification C 36.)

5) *Paint, latex*—coating of water-based paint consisting of one coat primer and one coat finish. The paint was white in color and applied with a brush. The exterior latex paints contained a fungicide to discourage the growth of mildew fungi.

6) *Paint, oil*—coating of oil-base paint consisting of one coat primer and one coat finish. The paint was white in color and applied with a brush. The exterior oil paints contained a fungicide to discourage the growth of mildew fungi.

7) *Pine, sugar*— 19.1 mm ($^3/_4$ in.) clear (i.e., no knots) planks of sugar pine 324-mm-wide, for tongue-in-groove siding.

8) *Plywood, fir*—12.7 mm ($^1/_2$ in.) rigid board for exterior sheathing comprised of five layers of thin sheets of wood (group 1, grade A-C veneer) glued so that grains of adjacent layers were at right angles.

9) *Polyisocyanurate, foil-faced*—12.7 mm ($^1/_2$ in.) rigid board for exterior sheathing comprised of a cellular plastic foam core reinforced with laminated foil facers on both sides.

10) *Vinyl plastic lapped siding*— white in color with a simulated wood-grain finish. Length: 3.4 m (135 in.) in increments of 127 mm (5 in.); Thickness: 1.0 mm (0.04 in.).

# APPENDIX B

## PERMEANCE MEASUREMENTS

### Thermal Insulation Materials

The permeance of the glass-fiber insulation was assumed to be equal to that of a stagnant air layer. This assumption is reasonable because the glass fibers of the insulation occupy a very small fraction of its volume. In this situation, it would be expected that bound-water diffusion along the glass fibers would be very small compared with molecular diffusion through the pore space. This assumption is supported by data contained in ASHRAE (1993) which shows that the permeability of mineral wool is very nearly the same as that for a stagnant air layer. A series of measurements, described below, were conducted to investigate whether the permeability is dependent upon the mean relative humidity across an air layer.

The experimental setup is depicted in Figure B-1 (a). Five precision-bore tubes, 3 mm in diameter and about 100 mm in length, were sealed into the top of glass vials. The vials were placed inside sealed glass vessels. Saturated salt-in-water solutions were used inside the glass vials and glass vessels to generate steady relative humidity environments at the lower and upper surfaces of the precision-bore tubes. For the five vial/vessel assemblies, the salt solutions given in Table B-1 were used to provide small differences in relative humidity of about 10 percent across the precision-bore tubes, covering the entire humidity range (fig. B-1 (b)). The measurements were conducted at an ambient temperature of 23.4 $\pm$ 0.1 °C.

**Table B-1**
**Relative Humidities[1] above Salt Solutions**

| No. | Salt Solutions | | Relative Humidities (%) | |
|---|---|---|---|---|
| | Vial | Vessel | Vial | Vessel |
| 1 | LCl | $KC_2H_3O_2$ | 11.30 | 22.74 |
| 2 | $MgCl_2$ | $K_2CO_3$ | 32.88 | 43.16 |
| 3 | NaBr | KI | 58.12 | 69.20 |
| 4 | NaCl | KCl | 75.36 | 84.59 |
| 5 | $Sr(NO_3)_2$ | $K_2SO_4$ | 85.66 | 97.39 |

[1] Equilibrium relative humidities above saturated salt solutions were taken from Greenspan (1977).

# PERMEABILITY TEST METHOD FOR FIBROUS INSULATIONS

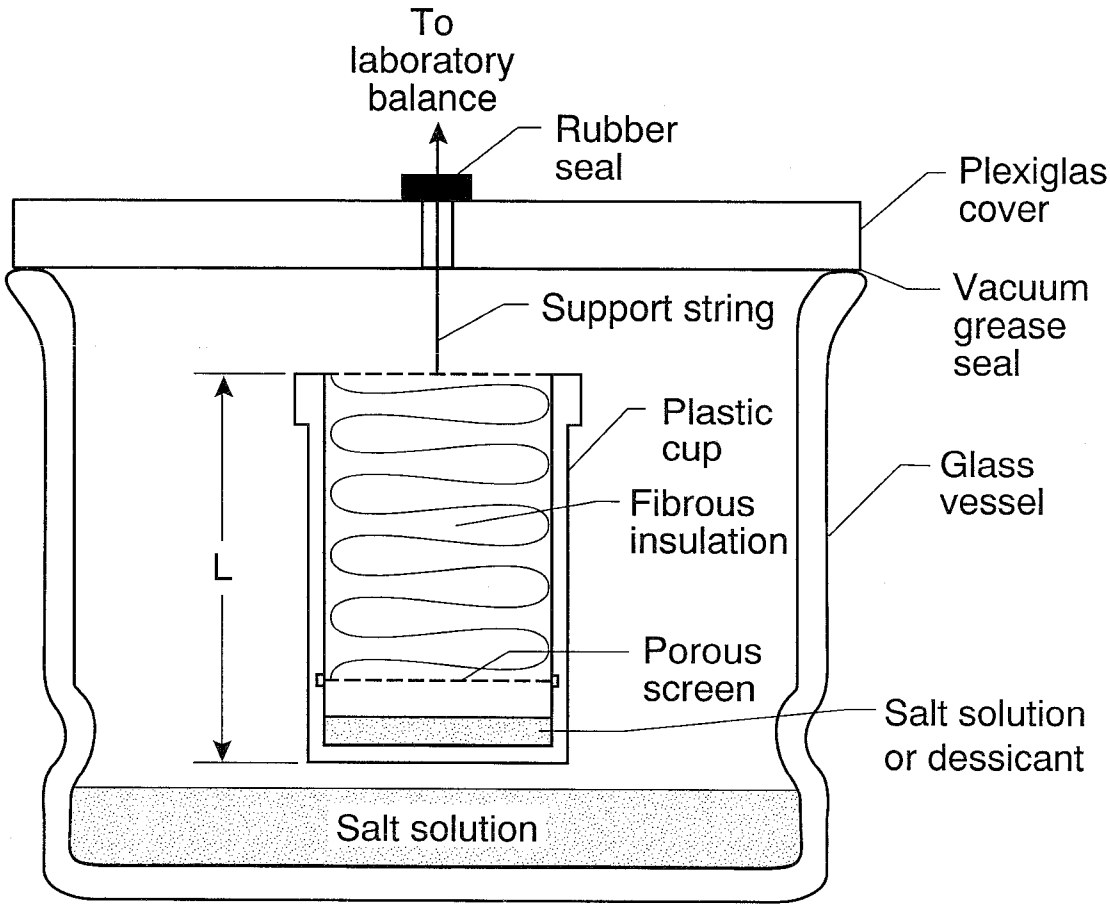


Experimental setup

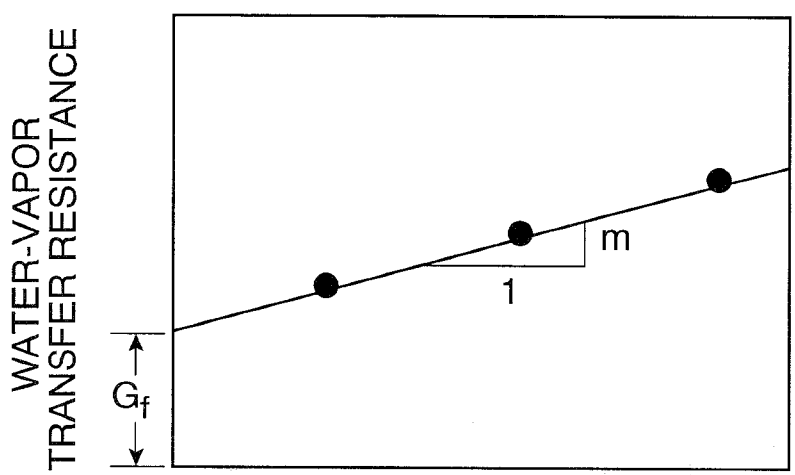


Analysis procedure

Figure B-1

The vials were weighed, placed in the glass vessels, and then weighed again at the end of a 2-month period. The water vapor transfer rate through the tubes was taken as the difference between the initial and final weights divided by the elapsed time. From Kreith (1968), the permeability may be determined from the relation:

$$w = A\mu\left(\frac{P_{atm}}{L}\right)\ln\left(\frac{P_{atm}-P_{gv}}{P_{atm}-P_{v}}\right) \qquad \text{(B-1)}$$

A plot of permeability measurements versus mean relative humidity is given in Figure B-2. The permeability is seen to be a constant value of $1.82 \times 10^{-10}$ kg/s·m·Pa and therefore does not depend on relative humidity. This permeability measurement agrees within 4 percent of the value published by ASHRAE (1993). The above permeability measurement of a stagnant air layer was also used for the cellulose insulation.

## Gypsum Wallboard

The permeance of gypsum wallboard was determined using three cup/vessel assemblies shown in Figure B-3. One sheet of gypsum wallboard was installed in the first cup, two (stacked) in the second cup, and three (also stacked) in the third cup. The measurements were conducted at a temperature of 21.4 °C. Magnesium-nitrate ($MgNO_3$) salt solutions were placed in the cups, while potassium-carbonate ($K_2CO_3$) salt solutions were placed in the glass vessels. The ambient relative humidity above the solutions of $MgNO_3$ and $K_2CO_3$ were measured using a precision dew-point hygrometer and found to be 51.3 percent and 42.5 percent, respectively. The interior surface of the gypsum wallboard faced the relative humidity of 51.3 percent. The water vapor transfer rate through the three specimens was determined by weighing the cups once a week as described above.

The total water vapor resistance, including the two air layers at the upper and lower surfaces of the specimen, was determined by the relation:

$$G_t = \frac{AP_g\Delta\phi}{w} + \frac{L}{1.75 \times 10^{-10}} . \qquad \text{(B-2)}$$

The last term of the above equation accounts for the reduction in the water vapor transfer resistance of the air layers due to the presence of the specimen.

The total water vapor resistance for the three cup/vessel assemblies was plotted versus the thickness of the specimen, as shown in Figure B-4. Again, the y-intercept at zero thickness represents the water vapor transfer resistance of the two air layers (extrapolated to a hypothetical zero thickness). The reciprocal of the slope (m) of this best-fit line is equal to a permeability of $6.38 \times 10^{-11}$ kg/s·m·Pa.

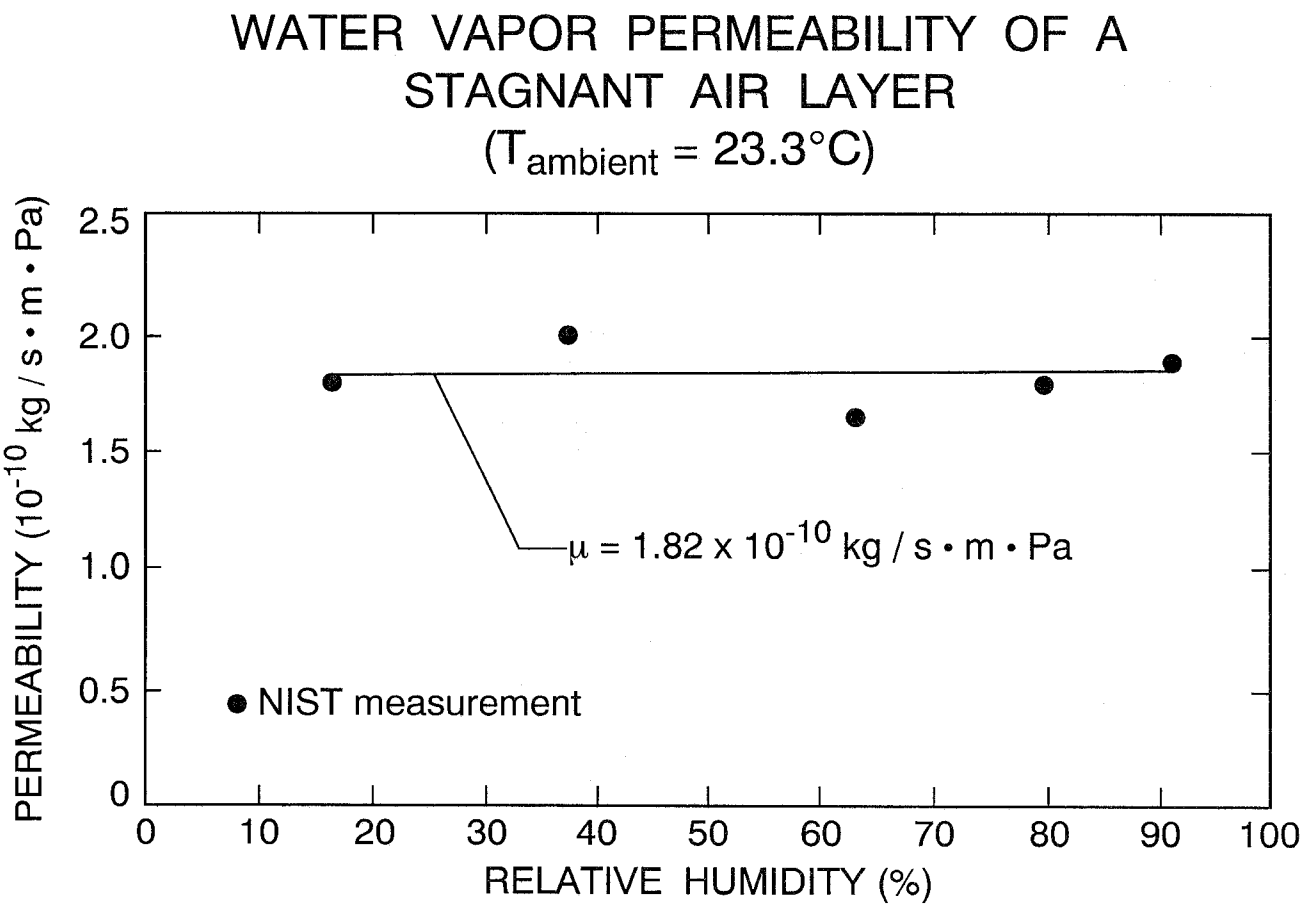
WATER VAPOR PERMEABILITY OF A
STAGNANT AIR LAYER
($T_{ambient}$ = 23.3°C)
PERMEABILITY ($10^{-10}$ kg / s • m • Pa)
2.5
2.0
1.5
1.0
0.5
0
0
10
20
30
40
50
60
70
80
90
100
RELATIVE HUMIDITY (%)
μ = 1.82 x $10^{-10}$ kg / s • m • Pa
NIST measurement

Figure B-2

# PERMEABILITY TEST METHOD FOR GYPSUM WALLBOARD

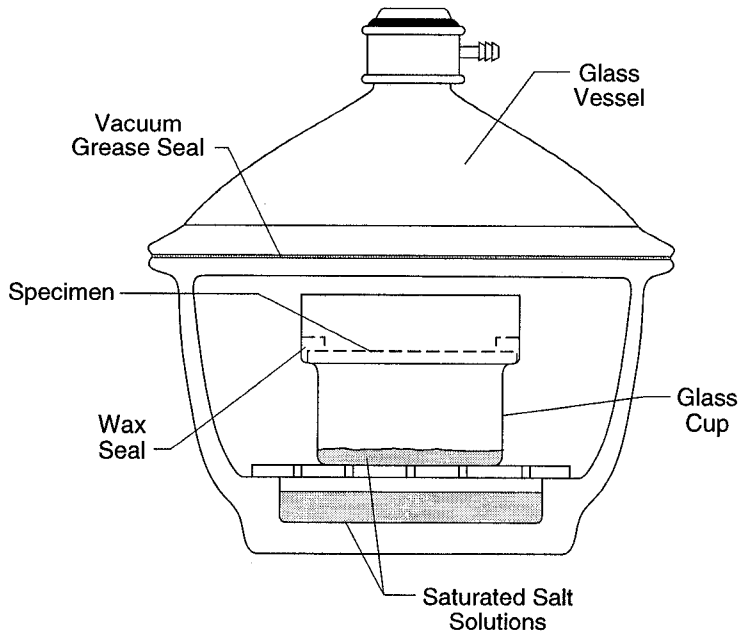


Experimental set-up.

Figure B-3

# WATER VAPOR TRANSFER RESISTANCE VERSUS THICKNESS FOR GYPSUM WALLBOARD

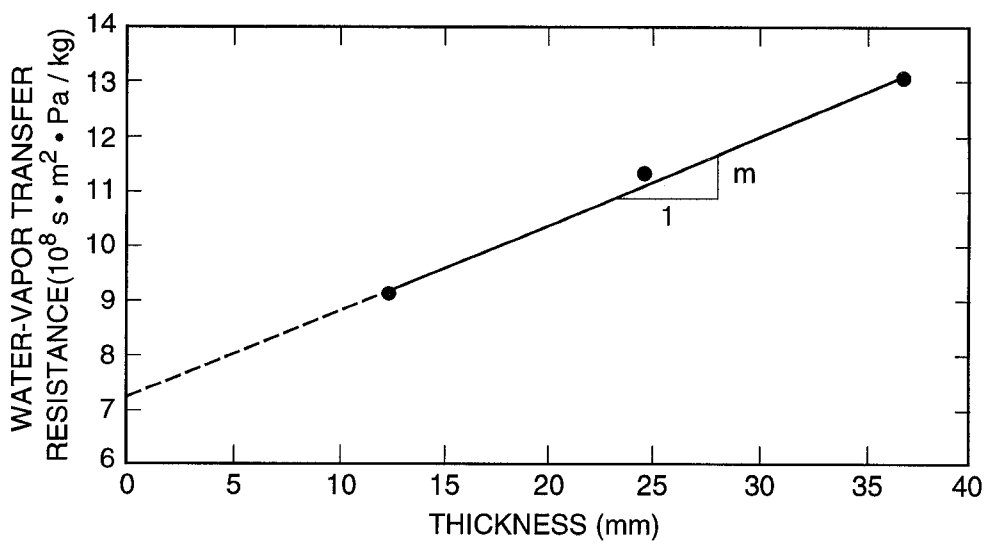


Figure B-4

## Paint Layers

*Latex Paint Applied to Gypsum Wallboard*

Four cup/vessels assemblies were prepared as shown in Figure B-3. A single layer of gypsum wallboard was installed in the first cup. The other three cups contained gypsum wallboard with the interior latex paint system (i.e., a primer and finish coat) applied to its interior surface. Note that the coatings of paint were applied at the same time as the wall specimens. The measurements were subsequently conducted as described above for the gypsum wallboard.

The total water vapor transfer resistance for each of the four cups was determined by eq (B-2). The resistance for each of the paint layers was determined by taking the difference in resistance between a cup with a latex paint and the cup without latex paint. The permeance of each of the paint layers is the reciprocal of its resistance. The permeance of the three paint layers was found to be $9.04 \times 10^{-10}$ kg/s·m²·Pa, $1.029 \times 10^{-9}$ kg/s·m²·Pa, and $1.00 \times 10^{-9}$ kg/s·m²·Pa. The average permeance is $9.77 \times 10^{-10}$ kg/s·m²·Pa.

*Oil and Latex Paint Applied to Sugar Pine*

Similar measurements were conducted to determine the permeance of the exterior latex and exterior oil-base paint systems. Both of the paint systems were comprised of a primer and finish coat. Three cup/vessel assemblies were prepared. The first cup contained a single layer of sugar pine. The other cups contained single layers of sugar pine with latex and oil-base paint systems applied. In this case, the measurements were carried out at a temperature of 6.7 °C. Potassium-acetate ($KC_2H_3O_2$) salt solutions were placed in the cups, while calcium-chloride ($CaCl_2$) desiccant was placed in the glass vessels. The ambient relative humidity above the solutions of $KC_2H_3O_2$ and $CaCl_2$ was 23.2 and 1.4 percent, respectively. The painted surfaces of the sugar pine faced the relative humidity of 1.4 percent. Applying the method above, the permeance of the latex and oil-base paint systems were found to be $1.9 \times 10^{-10}$ kg/s·m²·Pa and $8.04 \times 10^{-11}$ kg/s·m²·Pa, respectively.

## Convective Airspace

The water vapor permeance of the vertical airspace for specimen 7 was calculated using a modified form of the Lewis relation (Threlked 1970):

$$Le = 0.622 \frac{h_c}{h_w c_p P_{atm}} . \qquad \text{(B-3)}$$

Taking the Lewis number as 0.927, the convective conductance of the airspace as 2.00 W/m²·K, the specific heat of air as 1000 J/kg·K, and the atmospheric pressure as $1.01 \times 10^5$ Pa, the water vapor permeance of the vertical airspace was determined to be $1.33 \times 10^{-8}$ kg/s·m²·Pa.

☆ U.S. GOVERNMENT PRINTING OFFICE: 1995 - 386-627 - 814/37905